(2)

MECHANISTIC MODELS OF SOOT FORMATION

Annual Report

for

June 1991 to May 1992

Prepared by

M. B. Colket III
and
R. J. Hall

United Technologies Research Center

East Hartford, CT 06108

UTRC Report No. UTRC92-9

For

Air Force Office of Scientific Research
Bolling Air Force Base
Washington, D.C. 20332

Contract No. F49620-91-C-0056

J. M. Tishkoff

Program Manager

July 2, 1992

REPORT DOCUMENTATION PAGE

Form Approved
OMB No. 0704-0188

1. AGENCY USE ONLY (Leave blank)	2. REPORT DATE	3. REPORT TYPE AND DATES COVERED
	2 July 1992	Annual - 1 June 91 to 31 May 92

4. TITLE AND SUBTITLE

(U) Mechanistic Models for Soot Formation

5. FUNDING NUMBERS

PE - 61102F
PR - 2308
SA - BS
C - F49620-91-C-0056

6. AUTHOR(S)

Meredith B. Colket, III and Robert J. Hall

7. PERFORMING ORGANIZATION NAME(S) AND ADDRESS(ES)

United Technologies Research Center
Silver Lane
East Hartford, CT 06108

8. PERFORMING ORGANIZATION REPORT NUMBER

UTRC92-9

9. SPONSORING/MONITORING AGENCY NAME(S) AND ADDRESS(ES)

AFOSR/NA
Building 410
Bolling AFB DC 20332-6448

10. SPONSORING/MONITORING AGENCY REPORT NUMBER

11. SUPPLEMENTARY NOTES

12a. DISTRIBUTION/AVAILABILITY STATEMENT

Approved for public release; distribution is unlimited

12b. DISTRIBUTION CODE

13. ABSTRACT (Maximum 200 words)

One percent toluene in argon was pyrolyzed in a single-pulse shock tube coupled to a new GC/MSD analytical system. Many high molecular weight species were identified and this information is being used to examine and compare PAH formation mechanisms. Ring formation mechanisms during the oxidative pyrolysis of methane were compared and the dominant pathway was found to be recombination of propargyl radicals. Using an appropriately simplified reaction set, benzene profiles were predicted for the case of an opposed-jet, methane-air diffusion flame. A soot model was updated to include effects from particle ageing. A band radiation model was developed to treat radiation from flames with varying degrees of optical thickness. This code was used to model the effects of radiation from gas-phase species in a flame but can be extended to the case of particle radiation.

14. SUBJECT TERMS

Soot Formation Modeling, Band Radiation, Toluene pyrolysis, Formation and thermodynamics of polycyclic hydrocarbons, Ring Formation

15. NUMBER OF PAGES

74

16. PRICE CODE

17. SECURITY CLASSIFICATION OF REPORT	18. SECURITY CLASSIFICATION OF THIS PAGE	19. SECURITY CLASSIFICATION OF ABSTRACT	20. LIMITATION OF ABSTRACT
Unclassified	Unclassified	Unclassified	UL

UTRC92-9

MECHANISTIC MODELS FOR SOOT FORMATION

Annual Report

Table of Contents

List of Figures

List of Tables

UTRC92-9

MECHANISTIC MODELS FOR SOOT FORMATION

Annual Report

Summary

One percent toluene in argon has been pyrolyzed in a single-pulse shock tube coupled to a new GC/MSD analytical system. Many high molecular weight species have been identified, and this information is being used to examine and compare PAH formation mechanisms. Ring formation mechanisms during the oxidative pyrolysis of methane have been compared and the dominant pathway has been found to be recombination of propargyl radicals. Using an appropriately simplified reaction set, benzene profiles have been predicted for the case of an opposed-jet, methane-air diffusion flame. A soot model has been updated to include effects from particle ageing. A band radiation model has been developed to treat radiation from flames with varying degrees of optical thickness. This combined code has been used to model the effects of radiation from gas-phase species in a flame but can be extended to the case of particle radiation.

I. Introduction

The overall goal of this three year effort is to incorporate a soot model into a code for a laminar, opposed-jet, diffusion flame. Specific objectives necessary to reach this goal are: (1) identify reduced kinetic mechanisms which adequately describe ring formation and growth processes, (2) obtain and interpret new data on polyaromatic hydrocarbons (PAH) formed during hydrocarbon pyrolysis, (3) refine and update an existing soot formation model, (4) incorporate a radiation model into a code describing a laminar, opposed-jet diffusion flame, (5) incorporate the soot model into the flame code, and (6) identify simplification procedures such that solutions to this revised code can be achieved using easily obtained computer resources. In this first annual report, progress related to the first five of these items is briefly described.

II. Results

II. A. Reduced Kinetic Mechanism for Ring Formation

As part of the effort to develop a model for soot production in an opposed-jet diffusion flame, the reaction kinetics and mechanisms associated with ring formation during oxidative pyrolysis of methane must be established. Using data and a kinetic model developed in another program, the amount of benzene produced during oxidative pyrolysis of methane has been calculated. Several ring formation pathways are included in this model: $C_2H_x+C_4H_y$, $C_3H_x+C_3H_y$, and $C_5H_x+CH_3$. As shown in Figs. 1 and 2, the kinetic model adequately reproduces the major product species observed during the single-pulse shock tube oxidative pyrolysis of methane. In Fig. 2, note the reasonable agreement of the model with the experimental benzene profile. The contribution from each of the possible reaction paths to benzene was calculated and the dominant steps are plotted in Fig.

Figure 1

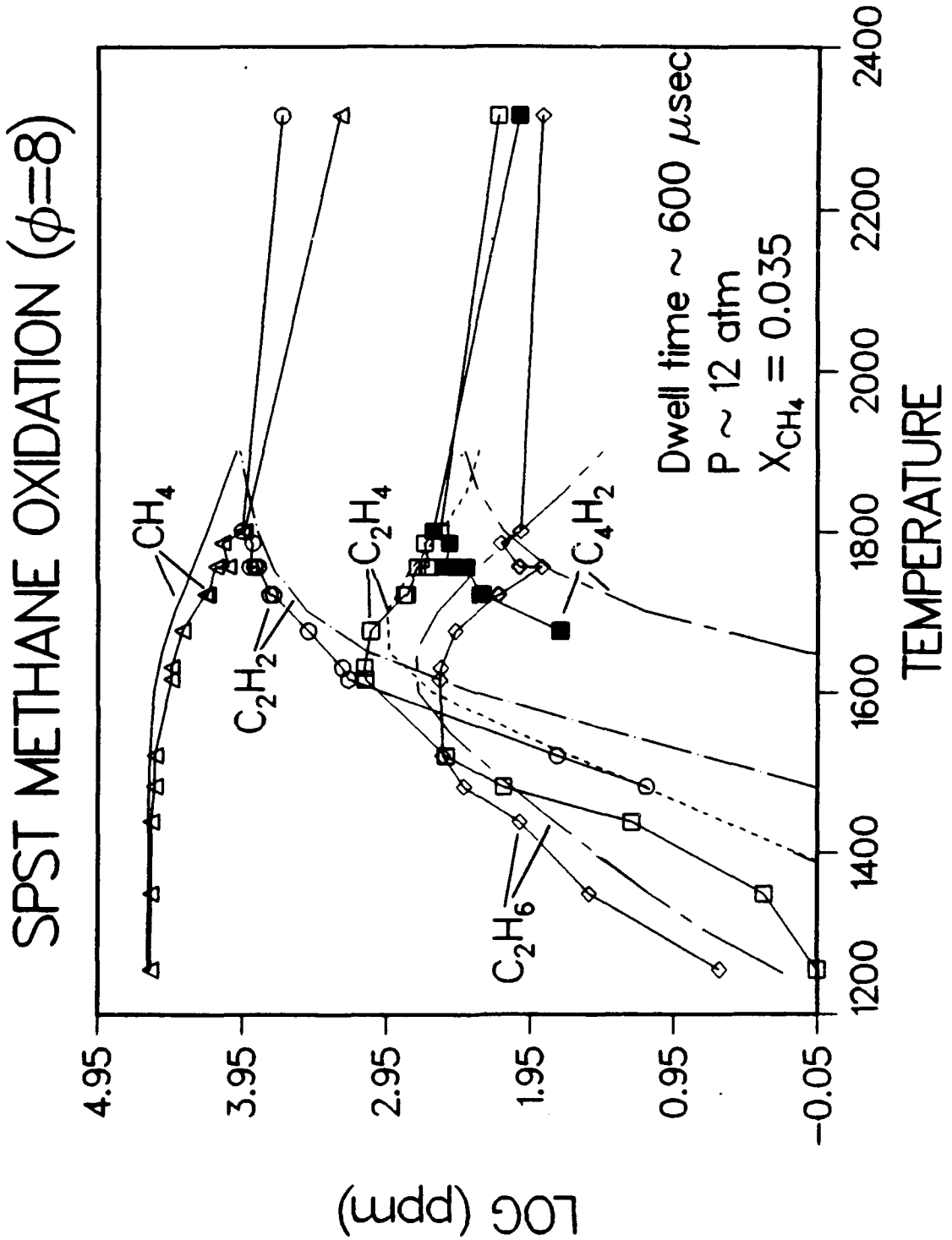
SPST METHANE OXIDATION (φ=8)
LOG (ppm)
4.95
3.95
2.95
1.95
0.95
-0.05
1200
1400
1600
1800
2000
2200
2400
TEMPERATURE
Dwell time ~ 600 μsec
P ~ 12 atm
X_{CH_4} = 0.035
CH_4
C_2H_2
C_2H_4
C_2H_6
C_4H_2

Figure 2

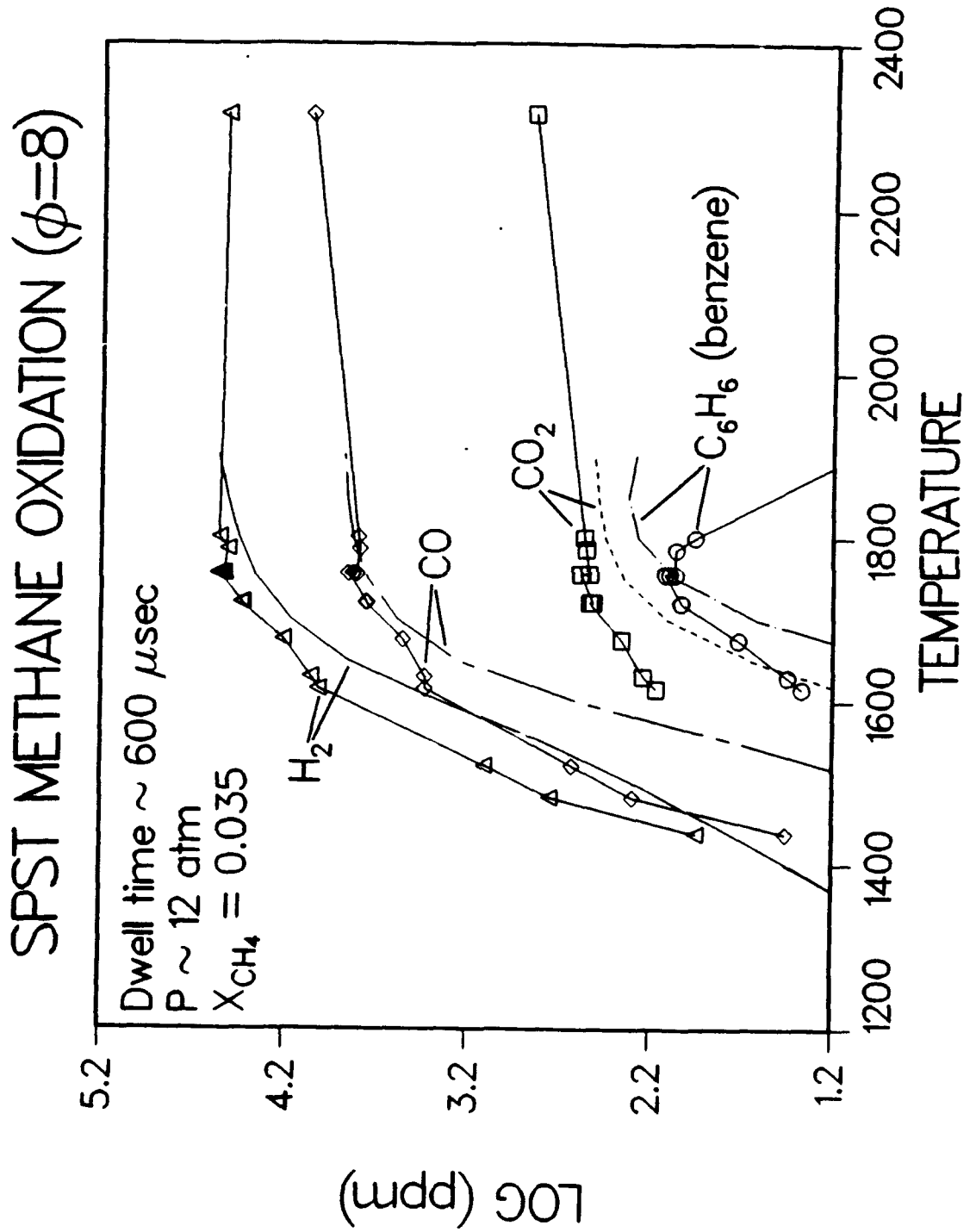
SPST METHANE OXIDATION (ϕ=8)
Dwell time ~ 600 μsec
P ~ 12 atm
X_{CH_4} = 0.035
H_2
CO
CO_2
C_6H_6 (benzene)
LOG (ppm)
5.2
4.2
3.2
2.2
1.2
1200
1400
1600
1800
2000
2200
2400
TEMPERATURE

3. The C_3H_3 recombination was found to be the strongly dominant pathway under high temperature, partial oxidation conditions. For these simulated single-pulse shock tube conditions, elapsed time is ~600 microseconds. The practical importance of this result is that (at least in diffusion flame calculations) only the kinetic processes associated with the C_3-mechanism need to be included in the otherwise complex model.

Based on these results, a reduced kinetic mechanism for the growth above C_2-species and the oxidation of aromatics (under oxidative pyrolytic conditions) was constructed. This set of seven additional species and 15 additional reactions is shown in Table I, and has been added to the kinetics mechanism that provides the solution for an opposed-jet, laminar, methane-air diffusion flame which includes C_2-chemistry. Estimated peak concentrations of the new species and gaussian profiles around the peak (initially located at 1700K, on the rich side) were used to accelerate convergence to a new solution with the added species and reactions. A calculated benzene profile for an opposed-jet, methane flame is shown in Fig. 4. The unusual minimum in the benzene profile (at peak temperature) is presumably due to the exclusion of oxidative reactions such as O or OH + benzene. Future modeling of such systems will include these reactions.

TABLE I

Preliminary Sub-Mechanism for Formation and Destruction of Benzene

($k_{forward} = A \exp(-E/RT)$)

	Reactions Considered	$\log_{10}A$ (cc-mole-sec)	E (kcal/mole)
1.	$C_3H_4+H \leftrightarrow C_2H_2+CH_3$	13.60	2.4
2.	$C_3H_4+H \leftrightarrow C_3H_3 + H_2$	12.00	1.5
3.	$CH_3+C_3H_4 \leftrightarrow C_3H_3 + CH_4$	12.30	7.7
4.	$C_3H_3+C_3H_3 \leftrightarrow$ PHENYL + H	12.70	0.0
5.	$C_6H_6+H \leftrightarrow$ PHENYL + H_2	14.40	16.
6.	$C_6H_6 \leftrightarrow$ PHENYL + H	16.70	107.9
7.	PHENYL + $CH_4 \leftrightarrow C_6H_6 + CH_3$	12.47	5.0
8.	PHENYL $\leftrightarrow$ *l*-C_6H_5	13.54	65.
9.	*l*-$C_6H_5 \leftrightarrow C_4H_3 + C_2H_2$	14.00	36.
10.	PHENYL + $O_2 \leftrightarrow$ c-C_5H_5 + CO + O	12.32	7.5
11.	c-$C_5H_6 \leftrightarrow$ H + c-C_5H_5	15.30	81.
12.	H + c-$C_5H_6 \leftrightarrow H_2$ + c-C_5H_5	12.47	8.0
13.	H + c-$C_6H_6 \leftrightarrow C_2H_4 + C_3H_3$	12.70	18.
14.	CH_3 + c-$C_5H_6 \leftrightarrow CH_4$ + c-C_5H_5	12.70	5.0
15.	c-$C_5H_5 \leftrightarrow C_2H_2+ C_3H_3$	14.00	74.

II. B. New Data on PAH Formation

Toluene (1% in a bath of argon) has been pyrolyzed in a single-pulse shock tube over

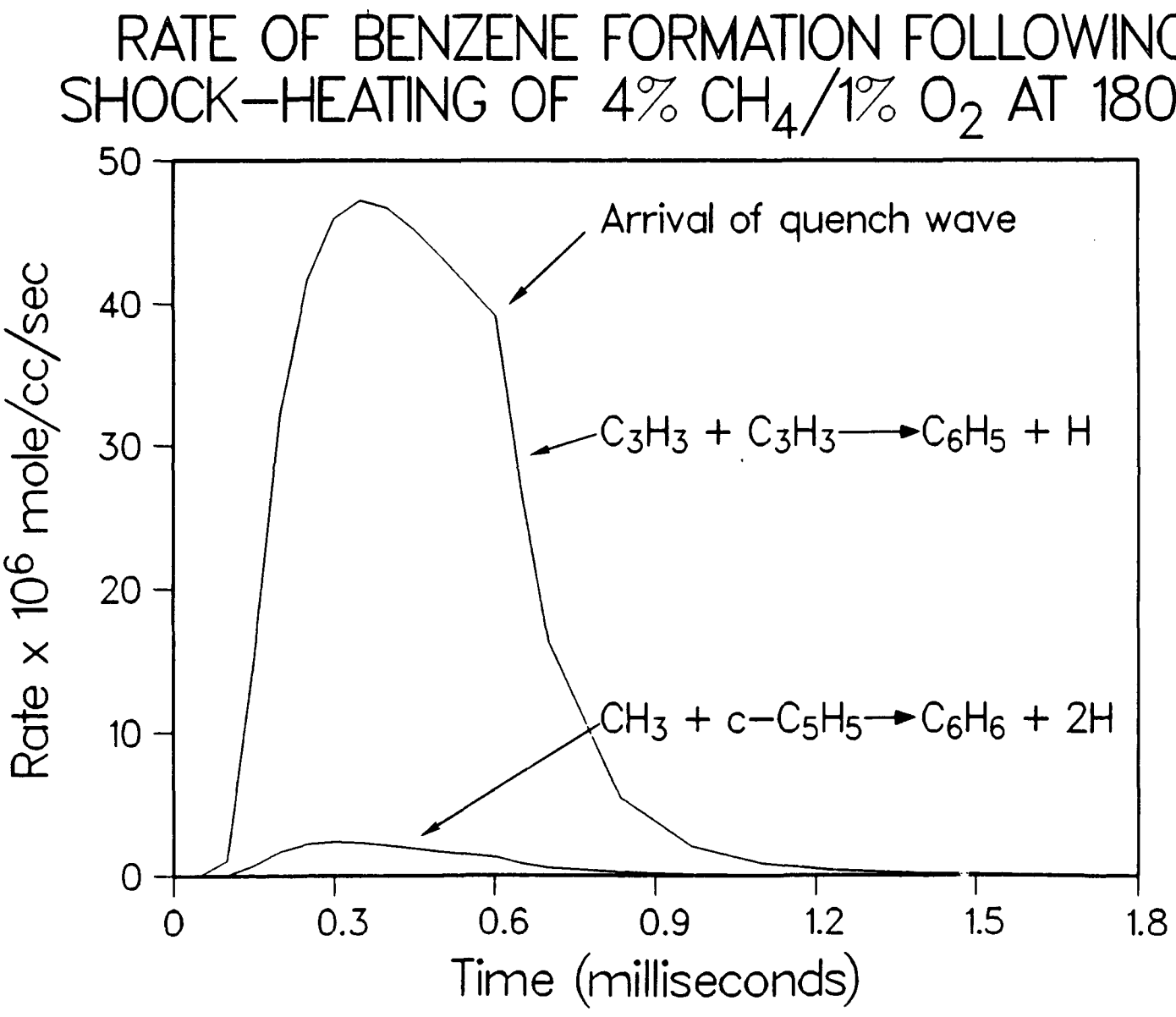
RATE OF BENZENE FORMATION FOLLOWING SHOCK–HEATING OF 4% CH_4/1% O_2 AT 1800K
Rate x 10^6 mole/cc/sec
50
40
30
20
10
0
Arrival of quench wave
$C_3H_3 + C_3H_3 \rightarrow C_6H_5 + H$
$CH_3 + c\text{–}C_5H_5 \rightarrow C_6H_6 + 2H$
0
0.3
0.6
0.9
1.2
1.5
1.8
Time (milliseconds)

Figure 3

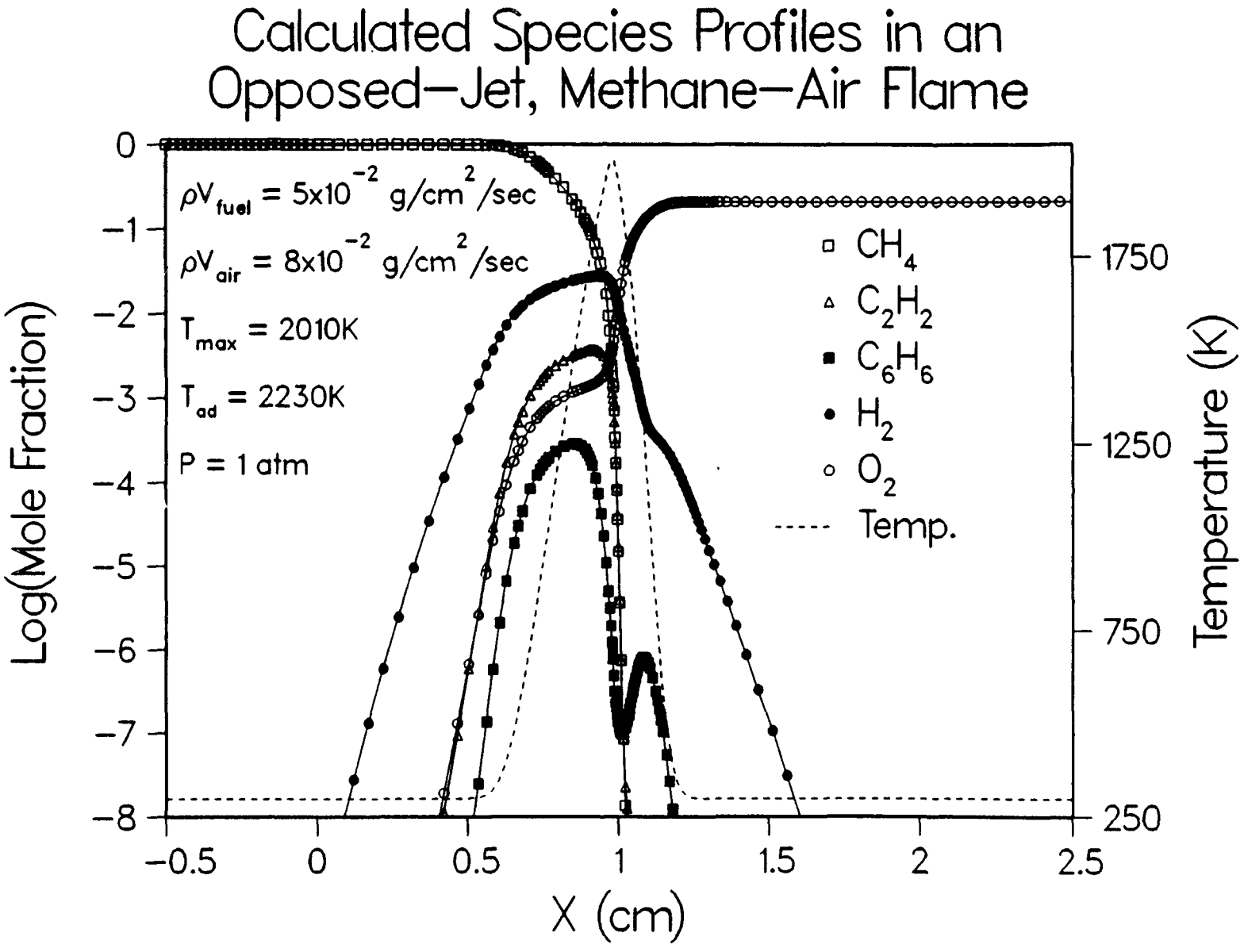
Calculated Species Profiles in an Opposed–Jet, Methane–Air Flame
ρV_{fuel} = 5x10^{-2} g/cm^2/sec
ρV_{air} = 8x10^{-2} g/cm^2/sec
T_{max} = 2010K
T_{ad} = 2230K
P = 1 atm
CH_4
C_2H_2
C_6H_6
H_2
O_2
Temp.
Log(Mole Fraction)
Temperature (K)
X (cm)
0
−1
−2
−3
−4
−5
−6
−7
−8
1750
1250
750
250
−0.5
0
0.5
1
1.5
2
2.5

Figure 4

the temperature range of about 1200 to 2000K and total pressures of 7 to 10 atmospheres. Products have been analyzed using a gas chromatograph coupled to a HP5971A mass spectrometric detector (MSD). Mass information has been obtained on species with molecular weights as high as 228 amu. Identification of species has been based on comparison to library standards and interpretation of cracking patterns. Modeling, speculation on reaction processes, and comparisons to literature have helped identify most of the species. A total of over 100 individual peaks have been detected, and the structure of more than 80 of these has been identified. Probable identifications have been made for most of the remaining trace species. Data is consistent with previous results[1] on toluene pyrolysis and confirms the tentative identification of product species. Table II lists many of the more dominant high molecular weight product species, their peak molar concentrations, and the approximate temperatures at which each peak concentration is found. The species listed in Table II are similar to those found[2] in a rich benzene flame, as well as those produced during lower temperature pyrolysis of toluene (see Smith[3]). Not only can the data obtained from pyrolysis experiments be used to examine growth processes, it can be also used to support proposed mechanisms for decomposition of toluene. For example, consider the low temperature products, cyclopentadiene and benzyl-cyclopentadienyl. These products strongly support arguments that c-C_5H_6 is an important intermediate following the decomposition of benzyl.

The recent results support the previous results showing early formation of bibenzyl and fluorene. Bibenzyl is formed via benzyl radical recombination. A proposal has been made[1] for the early formation of fluorene involving addition of a benzyl radical to benzene. Many of the previously unidentified peaks produced at low temperatures are methyl-biphenyl species, intermediates in the proposed fluorene formation mechanism. These results, as well as the identification of the benzyl-cyclopentadienyl species, strongly support the formation of high molecular weight species via ring-ring combinations. In addition, several high molecular weight, closed ring species with methyl or acetylene side chains were identified. Existence of these species also supports growth pathways involving addition of methyl radicals to rings and addition of aromatic radicals to acetylene. Kinetic modeling is planned, and results will be compared to the experimental data in an attempt to determine the relative importance of these different pathways. In order to perform kinetic modeling of this system, thermodynamic data on a variety of compounds containing five-membered rings is required. Limited information is available. Using literature values for indene, acenaphthylene, and fluoranthene, corrections (for five-membered rings) were estimated and used (together with group additivity techniques[4,5]) to predict thermodynamics for species such as fluorene, fluoranthene, and cyclopenta[def]phenanthrene. Thermodynamics of selected hydrocarbons are shown in Table III. Numbers in parentheses have been estimated in this work and the remaining data are from the literature[4,6-10]. Reactions associated with addition of acetylene to five-membered rings to form six-membered rings are discussed in Appendix A.

II. C. Inclusion of Ageing Effects into Existing Soot Formation Model

The soot formation model[11,12] has been extended to include an active site decay (ageing)

TABLE II
Products of Pyrolytic Decomposition of 1% Toluene

Name	Mass (amu)	Peak Concentration (ppm)	Temperature at Peak Concentration (K)
cyclopentadiene	66	20	1350
linear-C_6H_6	78	15	1350
benzene	78	1900	1550
phenylacetylene	102	260	1650
styrene	104	85	1450
ethylbenzene	106	60	1400
xylenes (3)	106	15	1450
indene	116	260	1650
methyl,ethynylbenzene	118	10	1650
diethynylbenzene	126	28	1650
ethenyl,ethynylbenzene	128	27	1650
naphthalene	128	800	1650
methylindene	130	10	1650
indenyl-acetylene	140	10	1600
methylnaphthalenes (2)	142	10	1650
acenaphthylene	152	250	1650
biphenyl	154	50	1550
benzyl-cyclopentadienyl	156	25	1350
fluorene	166	65	1500
phenalene (?)	166	12	1500
benzyl-phenyl isomers(6)	168	35	1400
phenanthrene	178	80	1600
anthracene	178	58	1550
(c&t)-stilbene	180	15,28	1450
bibenzyl	182	340	1350
bibenzyl isomers (7)	182	30	1400
cyclopenta[def]phenanthrene	190	10	1600
pyrene	202	20	1600
fluoranthene	202	11	1600
mass 202 isomers	202	3,10	1600
chrysene or triphenyl	228	7	1500

(n) - indicates n isomers detected; (?) - indicates uncertain identification

TABLE III
Thermodynamics of Selected Polycyclic Compounds

		$\Delta H^{\circ}_{f,298}$	S°_{298}	C_P (cal/mole/K)			
		(kcal/mole)	(cal/mole/K)	300	500	1000	1500
Indene	C_9H_8	39.1	80.7	29.6	48.3	73.4	83.9
Naphthalene	$C_{10}H_8$	36.0	79.7	32.3	52.5	78.5	89.4
Acenaphthylene	$C_{12}H_8$	61.6	86.7	36.1	59.2	88.8	100.0
Fluorene	$C_{13}H_{10}$	(47)	91.4	40.1	67.7	101.9	(114.9)
Phenanthrene	$C_{14}H_{10}$	50.0	94.5	44.9	72.8	107.2	121.2
Anthracene	$C_{14}H_{10}$	52.1	94.0	44.5	72.5	107.2	121.2
Cyclopenta[def]-phenanthrene	$C_{15}H_{10}$	(54)	(94)	(45.3)	(74.1)	(112.2)	(126.1)
Pyrene	$C_{16}H_{10}$	55.1	96.4	49.2	79.7	117.5	131.8
Fluoranthene	$C_{16}H_{10}$	69.8	(98)	(48.1)	(79.1)	(118.2)	(132.3)

Values in parentheses are estimated values.

term which slows the rate of surface growth at longer times. This modification was made since predictions of reductions in surface growth rates based on decay in H-atom concentrations inadequately described experimentally determined 'ageing' effects. Following the suggestion of Haynes[13], the surface density of active sites, denoted by χ, is allowed to decay with time according to

$$\frac{\chi}{\chi_o} = \exp\left(- \int_o^t k_{age}(T(t')) \, dt' \right) \tag{1}$$

where the decay rate constant is

$$k_{age} = 7 \times 10^6 \exp\left(- \frac{20,000}{T} \right) \text{ sec}^{-1} \tag{2}$$

and the time origin is the onset of net particle growth. The time-dependent value of χ can then be used with any of the several models of surface growth[11,12]. Inclusion of this term has an important effect in the simulations of high temperature soot growth, as shown in Fig. 5 for the acetylene and propane flames simulated[11,12]. The "modified Frenklach" growth mechanism, which gave the best overall agreement in the earlier studies, was used here. For

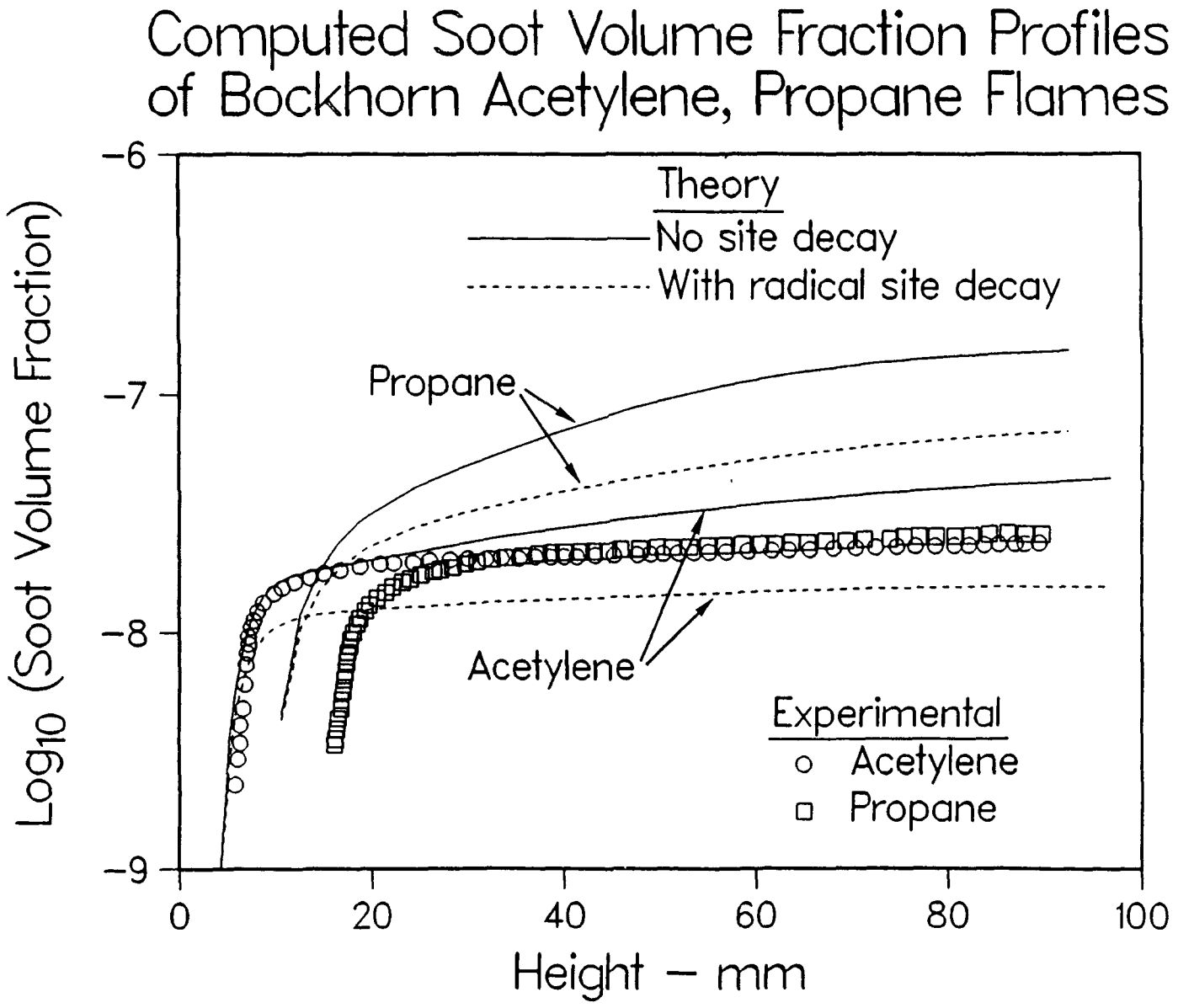
Computed Soot Volume Fraction Profiles
of Bockhorn Acetylene, Propane Flames
Theory
No site decay
With radical site decay
Propane
Acetylene
Experimental
Acetylene
Propane
Log10 (Soot Volume Fraction)
−6
−7
−8
−9
0
20
40
60
80
100
Height − mm

Figure 5

the acetylene flame, which is at the highest temperature, the predicted asymptotic growth behavior is now more consistent with experiment, as seen in the figure; although, the absolute magnitude is decreased. The lower temperature propane flame experiences a less drastic ageing effect in the simulation at long times, but the agreement with experiment is seen to be much improved. The ageing term is not as significant for the simulations of the lower temperature ethylene flames previously described[11,12]. Overall, inclusion of this effect has improved the theory-experiment comparisons. A lower overall activation energy than that shown in Eqn. (2) above should provide an even better comparison to the data.

II. D. Band Radiation Model

An objective of the current contract is to model radiative transfer effects in sooting counterflow flames. It was decided to approach the problem in an incremental fashion, first coupling gas band radiation alone to the counterflow solver. An expression for the radiant power density for gas band emission from H_2O, CO_2, and CO was derived based on wideband absorption models. The expression is derived from a solution to the radiative transfer equation for an infinite slab and is distinguished from other work in this area in being valid for any degree of optical thickness. Generally the optically thin limit is valid for higher strain rates, but finite optical thickness effects can become important at high pressure and very low strain rates. Nonadiabatic radiation loss from a flame will lower the peak temperatures and can appreciably affect predicted NO_x levels, for example. The radiant power density, which is equivalent to the divergence of the net radiative flux, has been included in the energy equation of a widely used counterflow code[14]. Thus a completely self-consistent analysis of the temperature reduction due to radiation and its effect on flame chemistry has been made. Details of the radiative algorithm are given in Appendix C, and radiative effects on predicted NO_x levels for conditions meant to simulate an aircraft gas turbine combustor have been described[15]. Sample calculations showing the effect of optical thickness on the local radiant power density are shown in Fig. 6 for a 10.5 atmosphere counterflow flame in which the methane fuel temperature has been chosen so that the adiabatic flame temperature approximates that of jet fuel. The base case strain rate is 56 sec^{-1}, and the lower strain rate cases have been generated by stretching the base case coordinates, assuming that characteristic lengths scale as (strain rate)$^{-0.5}$. All the cases in this figure employ the same converged temperature and species profiles from the adiabatic counterflow code for illustrative purposes. The nonadiabatic counterflow solver predicts that 1.75% of the total flame enthalpy release is converted to radiation at 56 sec^{-1}; at a strain rate of 20.5 sec^{-1}, it is predicted to rise to 4.5%. In sooting flames, the radiative losses are expected to rise significantly. The lower temperatures calculated when including band radiation have a substantial effect on prediction of emissions. Under the same conditions as for Fig. 6, NO levels have been calculated for opposed-jet flames and are plotted in Fig. 7 as a function of flame strain rate. These calculations include both 'thermal' and 'prompt' NO mechanisms, and indicate that inclusion of (gas-phase) radiation effects can reduce predicted NO emissions by as much as 30% under low strain conditions. Including effects of radiation from soot is expected to lead to even more dramatic results, since previous results indicate that 15-30% of the flame enthalpy can be lost via radiation from soot.

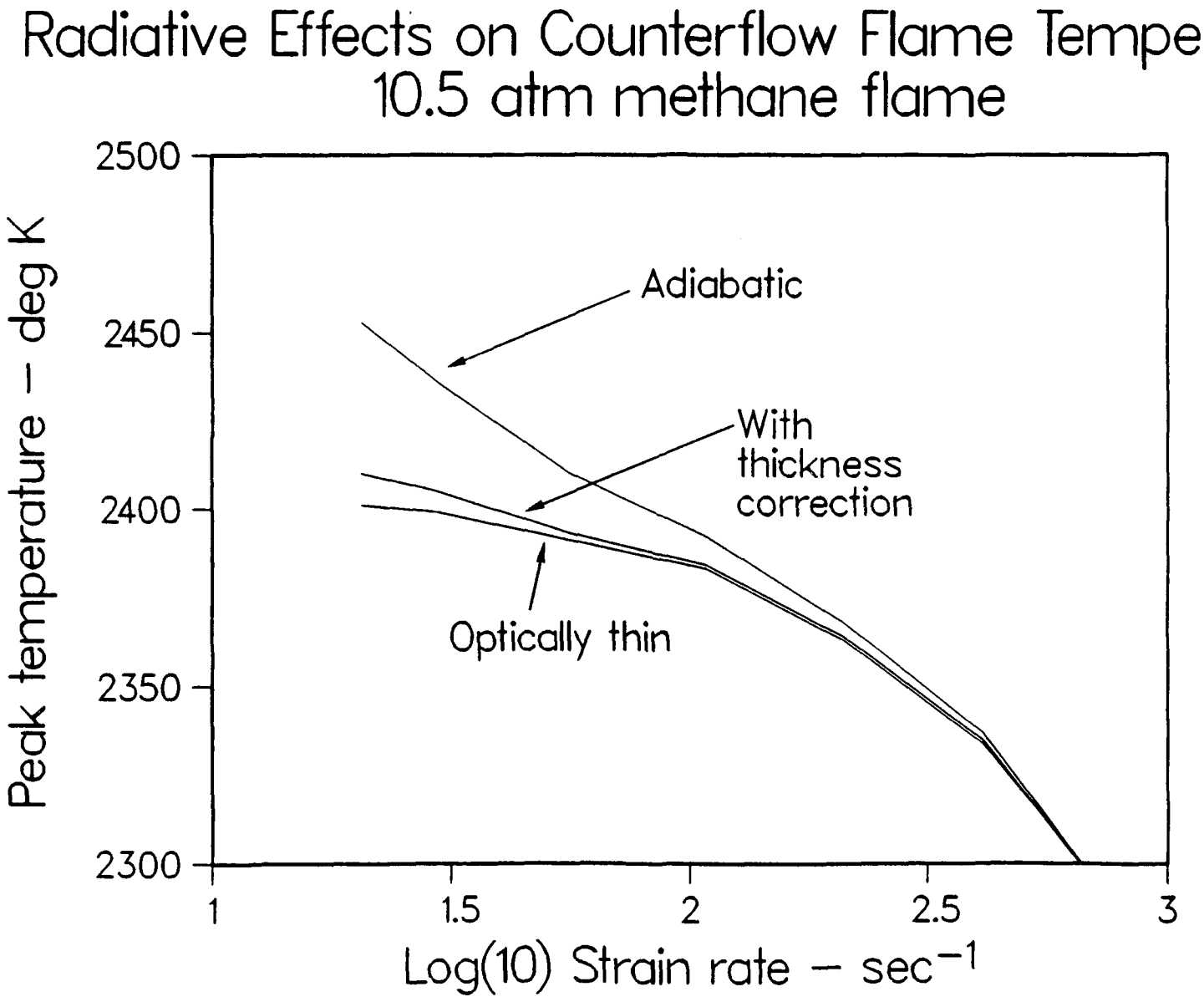
Radiative Effects on Counterflow Flame Temperature
10.5 atm methane flame
Peak temperature – deg K
2500
2450
2400
2350
2300
Adiabatic
With
thickness
correction
Optically thin
1
1.5
2
2.5
3
Log(10) Strain rate – sec^{-1}

Figure 6

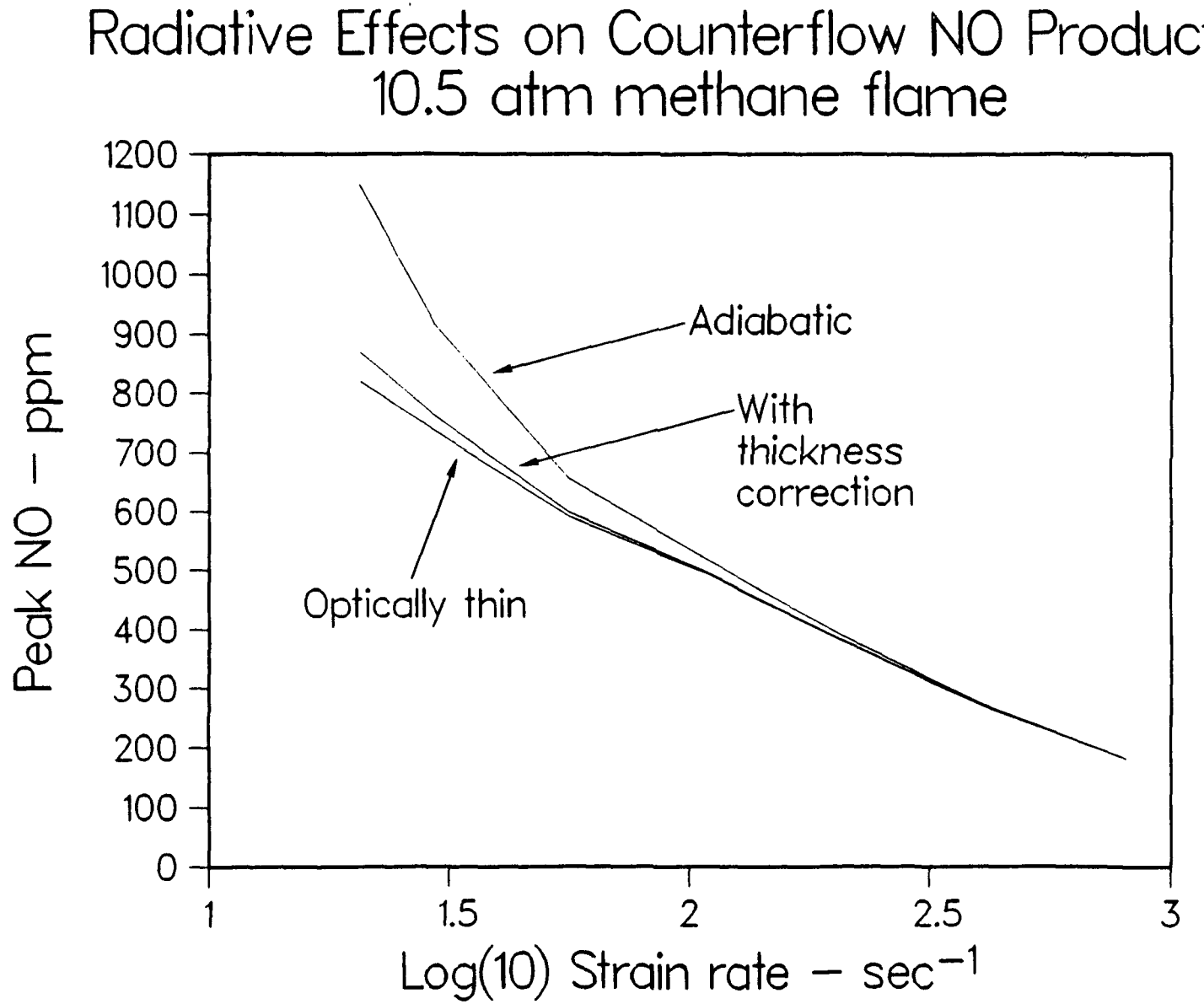
Radiative Effects on Counterflow NO Production
10.5 atm methane flame
Peak NO – ppm
1200
1100
1000
900
800
700
600
500
400
300
200
100
0
Adiabatic
With
thickness
correction
Optically thin
1
1.5
2
2.5
3
Log(10) Strain rate – sec^{-1}

Figure 7

Extension of the radiative model to include soot contributions should be a straightforward exercise. Professor M. Smooke of Yale University is assisting with the modifications of the opposed jet laminar flame code, and has extended his continuation analysis to radiation flames.

II. E. Formulation of Equations for Opposed Jet Flame Code

Species Conservation/Transport Equations for Sectional Analysis of Spheroid Growth

The dependent variables in the soot growth model are total mass densities within prescribed sectional boundaries, the boundaries being specified in particle mass,

$$Q_\ell = \int_{m_{\ell-1}}^{m_\ell} m n_\ell(m,r)dm \tag{3}$$

where n_ℓ is the intraclass particle density per unit particle mass. The MAEROS code assumes

$$n_\ell = \frac{Q_\ell}{m^2\ \ell n(\frac{m_\ell}{m_{\ell-1}})} \tag{4}$$

Instead of the Q_ℓ it is convenient to work with mass fractions Y_ℓ where

$$Y_\ell = \frac{Q_\ell}{\rho} = \frac{Q_\ell}{\rho_G + \sum_\ell Q_\ell} \tag{5}$$

The highest soot volume fractions observed in diffusion flames are $O(10^{-5})$. Thus,

$$10^{-5} \simeq \frac{\sum Q_\ell}{1.8} \rightarrow \sum Q_\ell \simeq 2x10^{-5} g/cm^3 \tag{6}$$

This could be approximately 10% of the gas density at flame conditions, meaning the soot mass can't be neglected in the total density calculation. The objective at this point is to start with the n_ℓ in deriving a conservation equation that is expressible in terms of the Y_ℓ. The species conservation equation for the n_ℓ in the standard counterflow coordinates[16] is,

$$\frac{1}{x}\frac{\partial}{\partial x}(x n_\ell u) + \frac{\partial}{\partial y}\left(n_\ell(v + v_T - \frac{D}{n_\ell}\frac{\partial n_\ell}{\partial y})\right) = \dot{n}_\ell \tag{7}$$

where v_T is the thermophoretic velocity and D the particle diffusion coefficient, respectively. Equation (7) is multiplied by m and integrated over m as in Equation (3), yielding (using $\frac{1}{x}\frac{\partial}{\partial x}(\rho u x) + \frac{\partial}{\partial y}(\rho v) = 0$)

$$\rho u \frac{\partial Y_\ell}{\partial x} + \rho v \frac{\partial Y_\ell}{\partial y} + \frac{\partial}{\partial y}\int_{m_{\ell-1}}^{m_\ell} m\left[n_\ell v_T - D\frac{\partial n_\ell}{\partial y}\right]dm = \dot{Q}_\ell \tag{8}$$

At this point, something must be known about the dependences of v_T and D on particle mass. For typical flame conditions, mean free paths will be order 5000-10000 $\AA$. Since soot spheroids will typically be 10-500 $\AA$ in diameter, one is unmistakably in the free molecule regime. Even a soot aggregate will rarely be larger than 1000 $\AA$. In this large Knudsen number limit, we have[17,18]

$$v_T = \frac{-3}{4}\,(1+\pi\,\alpha/8)^{-1}\,\left(\frac{\eta}{\rho_G}\right)\,\frac{1}{T}\,\frac{\partial T}{\partial y}$$

$$D = \frac{3}{2}\,\frac{KT}{d_p^2\,\rho_G\sqrt{\frac{2\pi\,KT}{m_i}}}\,(1+\pi\,\alpha/8)^{-1} \qquad (9)$$

$$= \frac{D'}{\rho_G/m^{2/3}}$$

where η is the gas viscosity, and both quantities have an accomodation coefficient α (thermal or momentum) that is near unity. The important point is that v_T is independent of particle size, and D is proportional to $m^{(-2/3)}$. Thus, the integrals in Equation 8 can be shown to be equal to

$$\rho u\,\frac{\partial Y_\ell}{\partial x} + \rho v\,\frac{\partial Y_\ell}{\partial y} + \frac{\partial(\rho Y_\ell v_T)}{\partial y} - \frac{\partial}{\partial y}\left(D_\ell\frac{\partial(\rho Y_\ell)}{\partial y}\right) = \dot{Q}_\ell \qquad (10)$$

where one uses the mass-weighted mean diffusion coefficient for the size class

$$D_\ell = \frac{\frac{3}{2}D'\left[m_{\ell-1}^{-2/3} - m_\ell^{-2/3}\right]}{\rho_G \ell n\left(\frac{m_\ell}{m_{\ell-1}}\right)} \qquad (11)$$

Defining a diffusion velocity

$$v_{D,} = -\frac{1}{\rho Y_\ell}\,D_\ell\,\frac{\partial(\rho Y_\ell)}{\partial y} \qquad (12)$$

the third and fourth terms on the l.h.s. of Equation (10) can be expressed as

$$\frac{\partial}{\partial y}\left(\rho Y_\ell\,(v_T + v_{D,})\right) \qquad (13)$$

The diffusion term may be important for the smallest (O(1nm)) soot particles. The right hand side of Equation 10 is the time rate of change due to aerosol processes, and can be expressed in terms of the Y_ℓ as

$$\dot{Q}_\ell = \frac{1}{2}\,\rho^2\,\sum_i\sum_j {}^{(1)}\beta_{ij\ell}\,Y_i Y_j - \rho^2 Y_\ell \sum_i {}^{(2)}\beta_{i\ell} Y_i$$

$$-\frac{\rho^2}{2}\,{}^{(3)}\beta_{\ell\ell}Y_\ell^2 - \rho^2 Y_\ell \sum_i {}^{(4)}\beta_{i\ell}Y_i + \rho\,{}^{(1)}G_\ell Y_\ell \qquad (14)$$

$$+\rho\,{}^{(2)}G_{\ell+\ell_n}Y_{\ell+\ell_n} - \rho\,{}^{(2)}G_\ell Y_\ell + \delta_{\ell 1}\,S(r)$$

where the growth and coagulation coefficients are as derived in Ref. 11.

III. List of Publications

A manuscript entitled "Successes and Uncertainties in Modeling Soot Formation in Laminar, Premixed Flames" by M. B. Colket, III and R. J. Hall has been written and will be published by Springer-Verlag in one of the "Springer Series of Chemical Physics". A copy of this paper is reproduced in Appendix B.

A manuscript entitled "The Radiative Source Term for Plane-Parallel Layers of Reacting Combustion Gases" has been prepared by R. J. Hall and has been submitted to Journal of Quantitative Spectroscopy and Radiative Transfer for publication. A copy of this document is provided in Appendix C.

A paper entitled "Influence of Radiative Loss on Nitric Oxide Formation in Counterflow Diffusion Flames at High Pressure" by A. Vranos and R. J. Hall is being prepared for submission to Combustion and Flame. Work specific to this manuscript has been funded by United Technologies Corporation; however, the study relies upon background work performed under the present contract.

IV. Meeting Interactions and Presentations

1. M. Colket attended an ARO Particulates Conference entitled "Particulates in Heterogeneous Combustors" on June 12-13, 1991 in Boulder, Colorado.
2. A workshop on "Mechanisms and Models of Soot Formation" was held in Heidelberg, West Germany on September 29 to October 2, 1991. The meeting was organized by Professor H. Bockhorn and was attended by about thirty-five engineers/scientists currently involved with understanding and modeling soot formation phenomena. Financial support was provided in part by VolkswagenStiftung and the Commission of the European Communities. M. Colket attended the meeting and presented a paper entitled "Successes and Uncertainties in Modeling Soot Formation in Laminar, Premixed Flames".
3. A paper entitled "Aerosol Dynamics Simulations of Soot Particle Growth in Flames" by R. J. Hall and M. B. Colket was presented at the 10^{th} Annual Meeting of the American Association for Aerosol Research, Traverse City, Michigan, October 7-11, 1991.
4. A paper entitled "A Soot Growth Mechanism Involving Five-Membered Rings" by M. B. Colket and R. J. Hall was presented at the Eastern Section of the Combustion Institute on October 14-16, 1991. The meeting was held at Cornell University in Ithaca, New York. A copy of this abstract is provided in Appendix A.

5. Department of Energy - Office of Basic Energy Sciences Combustion Research Meeting held at Tahoe City, California on June 15-16, 1992. M. Colket was invited by W. H. Kirchhoff to be an observer and participant at this D.O.E. contractor's meeting. The meeting was attended under corporate sponsorship.

6. M. Colket attended the second ARO Particulates Conference in Madison, Wisconsin on June 4, 1992. The objective of this meeting was to develop a method for planning a coordinated research program with the purpose of assisting the diesel industry in reaching legislated limits on emissions of NOx and particulates.

7. M. B. Colket presented an invited lecture entitled "Progress Towards Understanding Soot Formation and Development of Global Models" to the Diesel Cooperative Meeting held at United Technologies Research Center on May 17-18, 1990.

References

1. M. B. Colket, R. J. Hall, J. J. Sangiovanni, and D. J. Seery, "The Determination of Rate-Limiting Steps During Soot Formation", Final Report to AFOSR, Contract No. F49620-88-C-0051, August, 14, 1991. Also United Technologies Research Center report UTRC91-21.

2. J. D. Bittner and J. B. Howard, "Pre-Particle Chemistry in Soot Formation", in Particulate Carbon, Formation During Combustion, Ed. by D. C. Siegla and G. W. Smith, Plenum Press, New York, pp. 109-142, 1981.

3. R. D. Smith, "A Direct Mass Spectrometric Study of the Mechanism of Toluene Pyrolysis at High Temperatures", Journal of Physical Chemistry, Vol. 83, pp. 1553-1563, 1979.

4. S. E. Stein and A. Fahr, "High-Temperature Stabilities of Hydrocarbons," Journal of Physical Chemistry, Vol. 89., pp.3714-3725, 1985.

5. S. W. Benson, Thermochemical Kinetics, 2nd Edition, Wiley, New York, 1976.

6. A. P. Kudchadker and S. A. Kudchadker, "Indan and Indene",API Monograph Series, Publication 714, April, 1980.

7. J. Kao and N. L. Allinger, "Conformational Analysis. 122. Heats of Formation of Conjugated Hydrocarbons by the Force Field Method", Journal of the American Chemical Society, Vol. 99, pp. 975-986, 1977.

8. R. A. Alberty and A. K. Reif, "Standard Chemical Thermodynamic Properties of Polycyclic Aromatic Hydrocarbons and Their Isomer Groups. I. Benzene Series", Journal of Physical and Chemical Reference Data, Vol. 17, pp. 241-253, 1988.

9. R. A. Alberty, M. B. Chung, and A. K. Reif, "Standard Chemical Thermodynamic Properties of Polycyclic Aromatic Hydrocarbons and Their Isomer Groups. II. Pyrene Series", Journal of Physical and Chemical Reference Data, Vol. 18, pp. 77-109, 1989.

10. Z. U. Rehman and L. L. Lee, "Self Consistent Equations for Calculating Ideal Gas Heat Capacity, Enthalpy, and Entropy. III. Coal Chemicals", Fluid Phase Equilibria, Vol. 22, pp. 21-31, 1985.

11. M. B. Colket and R. J. Hall, "Description and Discussion of a Detailed Model for Soot Formation in Laminar, Premixed Flames," United Technologies Research Center, UTRC91-20, August, 1991. Also see Appendix A in Ref. 1.

12. M. B. Colket and R. J. Hall, "Successes and Uncertainties in Modeling Soot Formation in Laminar, Premixed Flames," presentation to the workshop on Mechanisms and Models of Soot Formation, Heidelberg, Germany, to be published in Springer Series of Chemical Physics, ed. H. Bockhorn, 1992. (see Appendix B)

13. B. T. Haynes, private communication, October, 1991.

14. M. D. Smooke, I. K. Puri, and K. Seshadri, "A Comparison Between Numerical Calculations and Experimental Measurements of the Structure of a Counterflow Diffusion Flame Burning Diluted Methane in Diluted Air," Twenty – First Symposium (International) on Combustion, The Combustion Institute, pp. 1783-1792, (1986).

15. A. Vranos and R. J. Hall, "Influence of Radiative Loss on NO_x Formation in Counterflow Diffusion Flames at High Pressure," to be submitted to Combustion and Flame, (1992).

16. V. Giovangigli and M.D. Smooke, "Extinction of Strained Premixed Laminar Flames with Complex Chemistry", Yale University Dept. of Mechanical Engineering Report ME-103-86, October, 1986.

17. S. K. Friedlander, "Smoke, Dust and Haze", Wiley, 1977, p. 31.

18. L. Waldmann, "Thermophoresis and Diffusiophoresis of Aerosols", in Aerosol Science (C.N. Davies Ed.), Academic Press, 1966, p. 140.

Appendix A

A Soot Growth Mechanism Involving Five-Membered Rings

A SOOT GROWTH MECHANISM INVOLVING FIVE-MEMBERED RINGS

by M. B. Colket and R. J. Hall
United Technologies Research Center
E. Hartford, CT 06108

Eastern Section: The Combustion Institute
October 14-16, 1991 at Ithaca, N.Y.

Conventional proposals regarding growth of polyaromatic hydrocarbons and soot particles focus on formation and growth of six-membered rings. Recently, the rapid conversion of five-membered rings to six-membered rings has been demonstrated in a single-pulse shock tube. Certainly, much of the work detecting polyaromatic hydrocarbons under soot forming conditions in flames demonstrates the presence of large concentrations of species containing five-membered rings. One can thus speculate that five-membered rings play a role in soot growth processes. It is the objective of this paper to examine the evidence and mechanisms for ring interconversions at elevated temperatures, to propose an alternative growth mechanism involving five membered rings and to compare that mechanism to a previous proposal for ring growth via six-membered rings.

Isomerizatiom processes causing ring enlargement and ring contraction are well known (Gajewski, 1981, Benson and O'Neal (1970), Ritter, et al., 1991). Ritter, et al. have recently examined the thermodynamics and kinetics of ring contraction, in particular conversion from a C_6-ring to a C_5-ring. To examine the possibility of ring enlargement, biacetyl (a source of methyl radicals) and acetylene have both been added (Colket, 1990) to the pyrolysis of cyclopentadiene (CPD). In the case of methyl radical addition, a dramatic increase in the formation of (the two isomers of) methylcyclopentadiene and benzene were observed. In the case of acetylene addition to CPD, dramatic increases in the formation of were observed. Colket did not discuss specific mechanisms for these processes, although the methyl addition steps are presumably similar to the reverse of the ring contraction processes outlined by Ritter, et al. Kiefer (1991) has suggested that the acetylene addition processes may be related to the reverse diels-alder reaction of acetylene addition to CPD to form norbornadiene. Benson and O'Neal (1970) report rates for unimolecular decomposition of norbornadiene to CPD plus acetylene and for the isomerization of norbornadiene to toluene. Thus one could speculate an overall process for ring enlargement:

$$C_5H_6 + C_2H_2 \leftrightarrow \text{norbornadiene} \leftrightarrow \text{toluene}$$

The overall rate constant for acetylene addition to CPD to form toluene can be estimated from our single-pulse shock tube (SPST) data. ($k = [\text{toluene}]_f/[\text{CPD}]_i/[C_2H_2]_i/t_{dwell}$). This data is plotted in Fig. 1 along with k_a for the reverse diels-alder reaction (obtained from detailed balancing and the rate data from Benson and O'Neal). A l.s.f. of the experimental data gives $k=10^{17}\exp(-58600$ cal/mole/R/T) cm^3/mole/sec. Although the SPST data is slightly higher than a extrapolation of the retro diels-alder rate constant at lower temperatures, the overall activation energy is significantly higher and the pre-exponential is about three orders of magnitude too large for a bimolecular process. We conclude that the dominant process observed in the SPST experiments is a radical process.

Based on the assumption of radical addition processes, we propose the reaction scheme in Fig. 2 as a possible alternative to a growth mechanism involving six-membered rings. The acetylene addition to cyclopentadienyl, formation of norbornadienyl, and isomerization to benzyl radical may be the reverse of a route for benzyl decomposition which has eluded researchers for years. Indene, formed in Reaction 7, has a five membered ring and, after loss of an H-atom (as in Reaction 1 or 2), it may undergo subsequent acetylene addition for further growth of polyaromatic hydrocarbons. Rewriting

this sequence as shown in Table I and assuming steady-state concentrations for all intermediate species, the expression for acetylene addition to 'soot' can be obtained:

$$\frac{d[C(s)]}{dt} = -\frac{2(k_1[H] + k_2)k_3k_4k_5[C_2H_2]^2[\text{cyclopentadiene}]}{(k_{-1}[H_2] + k_{-2}[H] + k_{1a})\{k_{-3}(k_{-4} + k_5) + k_4k_5[C_2H_2]\} + k_3k_4k_5[C_2H_2]^2}$$

Reaction 3 and -3 represents the overall reversible process of acetylene addition to cyclopentadienyl to form benzyl radical. Rate constants were initially determined based on literature values for these processes (with CPD) or estimates as necessary. An important difference of this new mechanism is the lower C-H bond strength in the C_5 ring species. The rate constant for acetylene addition to cyclopentadienyl was initially taken to be the reverse of that for the decomposition of benzyl radical. Rate constants were subsequently adjusted to provide better agreement to the soot growth data of Harris and Weiner (1983) and the soot growth rates studied by Bockhorn, et al. (1983) Final adjusted rate constants are shown in Table I where A-factors are in units of cm^3, moles, and seconds. Although these rate constants are relatively close to their initial values, these rates should be considered empirical and not directly related to processes with CPD or its derivatives. The overall soot growth rates as predicted by this equation are shown in Fig. 3 and 4 for the C/O = 0.96 and C/O = 0.80 ethylene flames of Harris and coworkers (1983 and 1988) respectively. Species concentrations were obtained as a function of height by using their kinetic model (Harris, Weiner and Blint, 1988) and the Sandia premixed code. Also shown on these figures are the experimental data and the predictions for soot growth via six-membered rings using the expression and rate constants as provided by Frenklach and Wang (FW) (1991). These predicted curves as well as those obtained using other assumptions (Colket and Hall, 1991) tend to peak early and are all concave upwards, whereas the experimental data is concave downwards. The shape of these 'theoretical' curves is at least partially due to their dependence on H-atom concentrations. For the richer flames, both of the calculated soot growth rates predicts the initial magnitude of the soot growth rate fairly well, although they both fall off too rapidly with increasing height above the burner. For the C/O=0.8 flame, the FW expression does not decrease by a factor of two (relative to the C/O=.94 flame) as the experimental data indicates and leads to substantial overprediction of soot formation in this leaner flame. As Frenklach and Wang explain, their expression, at the conditions in the Harris and Weiner flames, is proportional to H-atoms and independent of the acetylene concentration. Much of the prior work on soot growth including that of Harris and Weiner has been explained by a linear dependence of soot growth on acetylene concentrations. We believe that the inability of the FW expression to descibe the stoichiometric dependence of soot formation in the Harris and Weiner flames is at least partially due to the loss of the dependency on acetylene.

Soot profiles have also been predicted using these models. Both the FW model and this new model describe the soot profile for the C/O = 0.94 flame fairly well. The FW model significantly overpredicts the soot formation for C/O = 0.80 while this five-ringed model, slightly overpredicts soot production early in the flame. The five-ring model describes soot formation in the acetylene flame of Bockhorn without the 0.1 steric factor as suggested by FW. The new model significantly overpredicts (as does the FW model with the 0.1 steric factor) the propane data obtained by Bockhorn, et. al.

Acknowledgements

This work has been supported in part by the Air Force Office of Scientific Research under Contract No. F49620-88-C-0051. Special thanks are owed to Professor John Kiefer of the University of Illinois for valuable discussions on mechanisms of acetylene addition to cyclopentadiene.

References

S. W. Benson and H. E. O'Neal, Kinetic Data on Gas Phase Unimolecular Reactions, NSRDS-NBS 21, February, 1970.

H. Bockhorn, F. Getting, and H. W. Wenz, Ber. Bunsenges. Phys. Chem., 87: 1067(1983).

M. B. Colket, "The Pyrolysis of Cyclopentadiene", ES/CI, Dec., 1990.

M. B. Colket and R. J. Hall, "Successes and Uncertainties in Modeling Soot Formation in Laminar, Premixed Flames", workshop on Mechanisms and Models of Soot Formation, held at Heidelberg, Germany, Sept. 28 - Oct.2, 1991.

M. Frenklach and H. Wang, Twenty – Third Symposium (International) on Combustion, The Combustion Institute, p. 1559, 1990.

J. J. Gajewski, Hydrocarbon Thermal Isomerizations, Academic Press, New York, 1981.

S. J. Harris and A. M. Weiner, Comb. Sci. Tech., 32:267(1983).

S. J. Harris, A. M. Weiner, and R. J. Blint, Comb. Flame, 72:91(1988).

J. H. Kiefer, personal communication, 1991.

E. R. Ritter, J. W. Bozzelli and A. M. Dean, "Kinetic Study on Thermal Decomposition of Chlorobenzene Diluted in H_2", to appear in J. Phys. Chem.

Table I: Preliminary Soot Growth Mechanism Based on Five-Membered Rings

	Reactions Considered	$\log_{10}(A_f)$	E_f	$\log_{10}(A_r)$	E_r
1.	$H+C(s) \leftrightarrow \dot{C}(s)+H_2$	14.40	6	13.70	36
1a.	$\dot{C}(s) \rightarrow$ products	13.70	60	-	-
2.	$C(s) \leftrightarrow \dot{C}(s)+H$	14.78	86	14.48	-
3.	$C_2H_2+\dot{C}(s) \leftrightarrow \dot{C}'(s)$	12.04	12	12.00	70
4.	$C_2H_2+\dot{C}'(s) \leftrightarrow \dot{C}'(s)C_2H_2$	13.00	5	12.30	21
5.	$\dot{C}'(s)C_2H_2 \rightarrow \dot{C}''(s)+H$	11.4	5	-	-

Figure 1

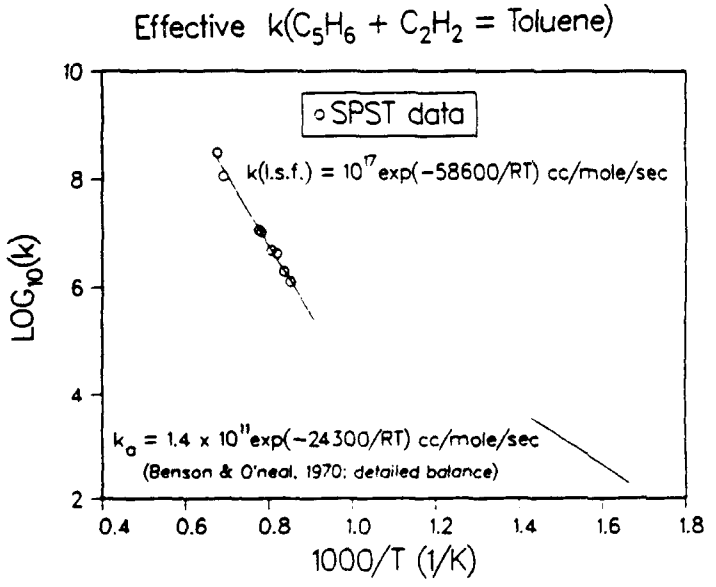

Figure 2: Alternate Ring Growth Mechanism.

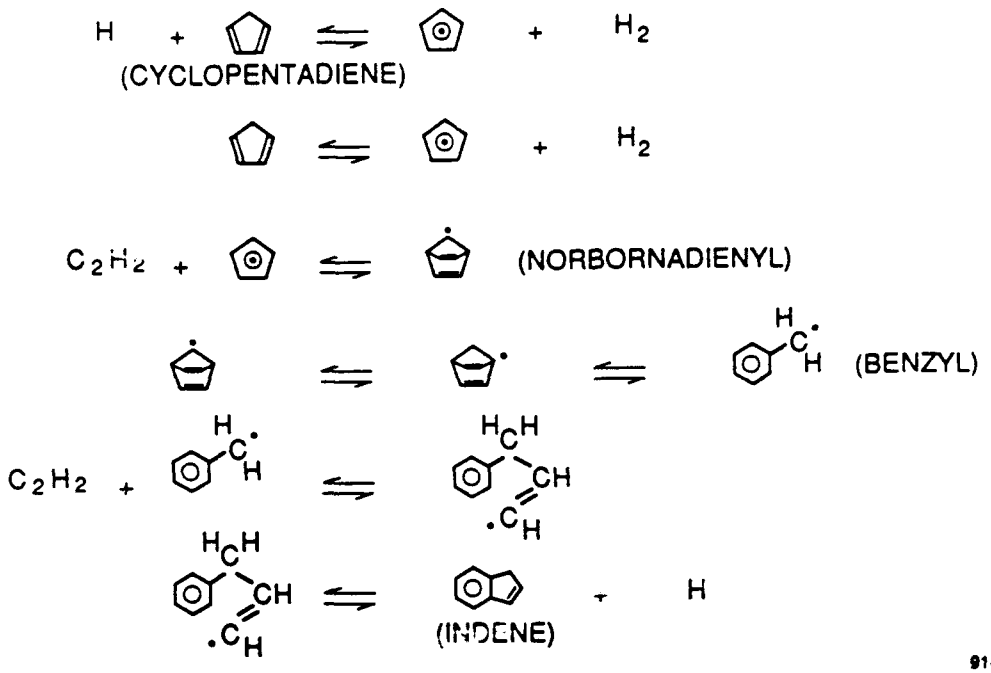

91-7-16-1

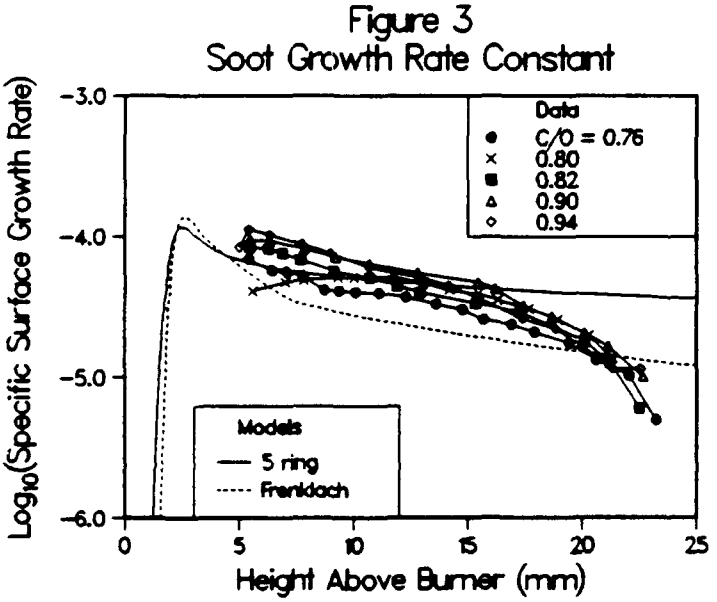

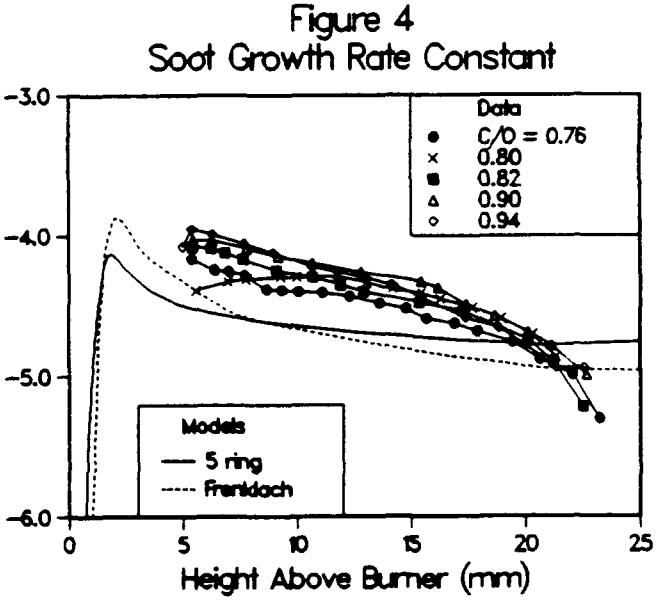

Appendix B

Successes and Uncertainties in Modeling Soot Formation in Laminar, Premixed Flames

SUCCESSES AND UNCERTAINTIES IN MODELING SOOT FORMATION IN LAMINAR, PREMIXED FLAMES

by

Meredith B. Colket, III and Robert J. Hall
United Technologies Research Center
East Hartford, CT 06108

presentation to the workshop on
Mechanisms and Models of Soot Formation

Heidelberg, Germany
September 30th to October 1st, 1991

to be published in
"Springer Series of Chemical Physics" (1992)

Abstract

A model for soot formation in laminar, premixed flames is presented. The analysis is based on a simplified inception model, detailed kinetic calculations of soot surface growth, and coalescing particle collisions. A sectional aerosol dynamics algorithm which involves solving a master equation set for the densities of different particle size classes provides an efficient solution scheme. The calculation of surface growth and coalescence sectional coefficients has been simplified and extended to the entire temperature range of interest in flame simulations. In order to test convergence properties, the former geometric limitation on the number of size classes has been relaxed. Convergence of the soot volume fraction typically requires only a few size classes and balance equations. Several possible soot surface growth models have been compared. The inception and surface growth models require profiles of temperature and important species like benzene, acetylene, and hydrogen atoms, and oxidizing species. Extensive comparisons have been made with well-characterized flame data by using experimental temperature profiles and calculating the concentrations of the important species with a burner code. Excellent agreement has been obtained with experimental species profiles where data are available. The calculated species concentrations and surface growth/oxidation rates are input to the aerosol dynamics program, which calculates the evolution of various soot size and density parameters. While aspects of the model are highly simplified, on balance it appears to give agreement with experiment that is comparable to that obtained from more elaborate models. The calculated sensitivity of soot growth to temperature and the important inception and coalescence parameters is discussed.

Introduction

The importance of soot production on pollution is well documented. In addition, soot formation can dramatically effect flame phenomena. The most obvious and acknowledged flame process affected by soot is radiation which can lead to substantial fractions of energy lost from the immediate flame environment [1, 2]. Twenty percent energy loss due to radiation is not atypical for a coflowing sooting diffusion flame [3]. This energy loss leads directly to a temperature reduction (and therefore affects kinetics of pollution formation), a change in density (and local gas velocity), as well as changes in flame length.

A secondary and often unrecognized phenomenon is the effect on flame thermochemistry and kinetics. The thermochemistry of soot formation and oxidation can dramatically affect the heat release profile in a flame. The conversion of alkanes, for example, to acetylene (a principal soot intermediate) is nearly one-fifth as endothermic as the oxidation process is exothermic. Thus, a strongly endothermic process can occur just inside the flame front to form soot. The soot may be transported to another region and oxidized. The oxidation rates of soot particles are dramatically different than those of gas-phase species. Local flame temperatures may be lowered in order to provide energy to drive the endothermic soot forming reactions. This process is also strongly dependent on fuel-type and often has not been considered by researchers addressing fuel-type effects on soot formation. The importance of the thermochemistry of fuel components is dramatically demonstrated in a recent analysis [4]. Their model indicates the existence of a region of negative heat release just below the apex of a coflowing diffusion flame! This effect is attributed principally to the strongly endothermic reaction, $2CH_4 = C_2H_2 + 3H_2$.

These flame effects are often so dominant that the modeling of practical (soot-containing) flames will be highly inaccurate without predictions of soot formation as part of the flame modeling process. Further support for modeling efforts comes from the more commonly recognized deleterious effects of soot formation, such as pollution, hardware lifetimes, and plume visibility.

Consequently, over the past several years a procedure for calculating soot production in one-dimensional laminar, premixed flames has been developed. This procedure has similarities with techniques developed at other laboratories [5, 6, 7]. It is hoped that this or similar procedure could be used for predicting soot in more complex flame systems. Although there are limitations and uncertainties with the developed code, the procedure is quite versatile and is quite successful in predicting soot production from several different laboratory flames. A detailed description for most of the calculation procedure is provided in this manuscript as well as a discussion of the principal assumptions, successes, and uncertainties. The formulation and modifications to the MAEROS code [8] as used in this soot model are described elsewhere [9]. Despite uncertainties, the code in its present form is a useful tool for evaluating the controlling soot formation processes in different flames and for providing valuable understanding to the many interrelated and competitive processes of soot formation. Examination of this soot model and its predictions leads to some increased understanding of the overall successes and uncertainties in soot formation modeling.

Brief Description of Model

A flow chart of the model used to describe soot formation processes is provided in Fig. 1. Dashed lines are used for portions of the code which have not yet been implemented. The model couples detailed chemical kinetics calculations of gas-phase processes with mechanisms for particle surface growth, oxidation, and agglomeration. MAEROS, a widely-used aerosol dynamics code [8], has been modified for the latter part of the analysis.

Figure 1 A soot growth model for a premixed, laminar flame

The soot growth/aerosol dynamics program is based on a sectional representation of the growth equations with provision for inception source terms, surface growth through condensible vapor deposition, and coagulation. The program has been modified in a number of ways for the soot growth problem. Its temperature range capabilities have been extended to the full range of interest in combustion problems by a reformulation of the surface growth and coalescence sectional coefficient calculations. Provision for oxidizing vapors (oxygen and hydroxyl radicals) has also been made. The simulations require as input profiles of temperature, aromatics (C_6H_6), condensible (C_2H_2) and oxidizing vapor concentrations (OH and O_2), and the concentrations of other flame species (such as H-atoms and H_2). The input of the aerosol dynamics program has been made compatible with the output of the Sandia premixed, laminar flame program [10, 11]. The facility to exclude small mass spheroids from coagulative processes has also been added. The code also calculates the radiative energy loss from soot assuming optical thinness and neglecting soot refractive index dispersion.

In the present version of the model, the inception calculation makes use of the local benzene formation rate. Starting with benzene, the surface growth process alone is used to generate small mass, solid carbon spheroids. At a specified threshold mass, particle coalescence is allowed; the inception rate is taken to be the flux of particles through this threshold mass, beyond which it is assumed that one is describing soot particles. This model of inception is based on an extrapolation of particle growth dynamics and kinetics into the pre-particle regime; although benzene is not the inception species, the particle dynamics calculations begin at a particle mass equivalent to the carbon content of benzene, with a source rate derived from the benzene formation rate. This simple, provisional assumption about inception may be just as good as those presently obtainable from more elaborate calculations of the inception species, given the uncertainties presently associated with the latter. As additional information becomes available, this assumption may be modified as required. The sensitivity of the results to the inception species mass will be discussed later in the text.

Acetylene is assumed to be the surface growth species. The growth rate has been calculated using the Harris-Weiner [12] value, the Frenklach-Wang expression [5], as well as several other steady-state expressions. Local values of acetylene and hydrogen atom/molecule concentrations as well as estimates of rate coefficients for certain kinetic processes are required for these calculations. Oxidation is assumed to be given by the Nagle and Strickland-Constable expression [13], and oxidation by OH by a gas kinetic rate multiplied by a collision efficiency of 0.13 [14]. Recent studies have shown that soot mass also grows by the addition of polyaromatic hydrocarbons. These processes are included in the present model since low molecular weight polyaromatic hydrocarbons are included in the total soot mass (according to the model used in this study) and these species are allowed to grow by acetylene addition as well as by coagulation with other 'soot' particles.

Modeling of Gas Phase Chemistry

In this investigation, extensive comparisons were made with the well-characterized, premixed, burner-stabilized flames examined by Harris and Weiner [12] and by Bockhorn, Fetting, and Wenz [15]. Concentrations of gas-phase species were calculated using detailed chemical kinetic models with CHEMKIN II [11] and the SANDIA premixed flame code [10]. The purpose of these calculations is to determine concentrations of gas-phase species as a function of height above the burner. These data in turn are used to calculate inception rates and specific growth rates. Thus far, experimentally determined temperature profiles have been used; in general, a code could calculate the temperature profile once radiation, thermodynamics of soot formation, and burner effects are included in the model. Results from the kinetic modeling efforts are described in the following para-

graphs. Since benzene has been assumed to be the incepting particle in the present calculations, the discussion is focused on the predictions of benzene profiles.

For the atmospheric pressure, $C_2H_4/O_2/Ar$ flames examined by Harris and Weiner [12], the kinetic code of Harris, Weiner and Blint [16] was used with the addition of the reaction

$$C_3H_3 + C_3H_3 \leftrightarrow C_6H_5 + H \qquad (1)$$

Recently, this and related reactions have been found to contribute significantly to benzene formation in rich flames. The rate constant for Reaction 1 was 10^{13} cm^3/mole/sec [17]. For the C/O = 0.92 flame, it contributes approximately 50% of the total formation of benzene.

For the low pressure acetylene (0.12 atm) and propane (0.15 atm) flames studied [15], species profiles were calculated using a modified version of the kinetic code of Miller and Bowman [18] with propane kinetics from Westbrook and Dryer [19]. (Numerical problems were encountered with the Harris kinetics.) The same ring-forming reactions used to model the Harris and Weiner flames were also included in this kinetic sequence. A sensitivity analysis on benzene formation in the acetylene flame indicates that, besides chain branching and termination steps, its formation is principally dependent on reactions linked to the formation and destruction of C_3H_3. These results support the recent findings in several studies [17, 20, 21] regarding the significance of C_3-species to benzene formation in flames. Our results which indicate the importance of Reaction 1 differ from the conclusions of Franklach and Wang [22]. It is likely that this difference is due in part to differences in the C_3-reaction set or related thermodynamics.

Calculated values for selected species are compared to experimental data in Colket and Hall [9]. In general, agreement is reasonable except for a spatial misalignment with the Bockhorn, et al data [15]. As described in Colket and Hall, the descrepancies are partly due to experimental uncertainties.

Simplified Inception Model: Justification and Motivation

The use of an incepting species derived from benzene, as explained previously, is justified by several facts. First of all, benzene has been found in this laboratory as well as by Kern, et al. [23] to correlate directly with sooting tendencies for a variety of aliphatic hydrocarbons; secondly, while relatively small uncertainties exist in our ability to predict benzene concentrations (factor of two), large uncertainties exist in the prediction of multi-ringed aromatics (probably a factor of ten or more), so calculations of inception based on concentrations of these high molecular weight species are at the present time subject to large error; thirdly, results can be very sensitive to the selection of the incepting species and its selection appears to be somewhat arbitrary; and fourthly, the actual mechanism for inception is not yet known (although some good speculation is available). Consequently, we conclude that there are significant uncertainties in calculating the true inception rate and, therefore, starting our particle growth calculation with benzene and defining the inception species to correspond to that particle mass at which coalescence begins is as good as other uncertain alternatives. As will be seen, use of this assumption yields reasonable agreement with experimental data in many regards.

In addition to these justifications, there is a strong motivation for using a simplified inception process. Calculation times for solutions of flame systems increase dramatically as the number of flame species increase. This concern becomes even greater as multi-dimensional flames are considered. Already, the calculation time for solution of the gas-phase kinetics (many hours) by far dominates over the solution times of the aerosol dynamics (seconds to a couple of minutes on an IBM 486 pc).

Soot Growth Mechanisms

Soot growth rates were calculated using a variety of procedures, each of which exhibit different features. Two literature 'mechanisms' were used, i.e., the Harris and Weiner (HW) expression [12] with an activation energy of 31.8 kcal/mole and the Frenklach and Wang (FW) mechanism [5]. In addition, three other mechanisms (MODFW, 8STEP, 5RING) have been developed [5]. For the latter four mechanisms, steady-state assumptions are made for all intermediate 'species' and expressions for overall soot growth rates were determined. In the latter three cases, rate constants were initially selected based on literature expressions but then adjusted (typically less than a factor of four) in order to provide better agreement with experimental data (that is, specific surface growth rates from Harris and Weiner and the soot profiles from Bockhorn, et al). Frenklach and Wang's approach of not altering rates from those which describe reactions for low molecular weight species is admirable. However, we justify our adjustments due to the fact that rate constants between low and high molecular weight species are not necessarily identical for similar processes (due to changes in molecular structures as well as reduced masses) and since a simplified sequence is used to describe what is probably a very complex process.

The soot growth rates do not employ the particle ageing equation [24] which reduces growth rates with increasing particle time. This process was not included in this study because of our initial acceptance of the arguments of Franklach and Wang [5] indicating that particle ageing was an artifact of the H-atom decay process. As described subsequently in this paper, this argument was found not to be consistent with experimental data. In future studies, equations for particle ageing will be included in the analysis; it can be expected that modifications to empirically derived rate constants used in this analysis will be necessary.

For simplification, only our modified Frenklach and Wang mechanism is described in this document. All mechanisms are described in Colket and Hall [9]. As an alternative to the multiplying factor of 0.1 required to explain the high temperature flame data of Bockhorn and coworkers, we attempted (Frenklach and Wang also tried a similar approach) to include some reversibility in the acetylene addition process. The resulting mechanism (MODFW) is listed below.

Table I: Modified Version of the FW Soot Growth Mechanism (MODFW)

	Reactions Considered	$\log_{10}(A_f)$	E_f	$\log_{10}(A_r)$	E_r
1.	$H+\dot{C}(s) \leftrightarrow \dot{C}(s)+H_2$	14.40	12	11.6	7.0
2.	$H+\dot{C}(s) \leftrightarrow C(s)$	14.34	-	17.3	109.
3.	$\dot{C}(s) \rightarrow$ products $+ C_2H_2$	14.48	62	-	-
4.	$C_2H_2+\dot{C}(s) \leftrightarrow C(s)\dot{C}HCH$	12.30	4	13.7	38
5.	$C(s)\dot{C}HCH \rightarrow C'(s)+H$	10.70	-	-	-

includes possible acetylene elimination from the soot radical (analogous to phenyl radical decomposition) and separates the acetylene addition process into a reversible formation of the radical adduct and a cyclization reaction. Assuming steady-state conditions for all intermediate species, the rate expression for soot mass growth is calculated to be

$$\frac{dm}{dt} = 2m_c \frac{(k_1[H] + k_{-2}[C_2H_2])k_4k_5\chi A}{(k_{-1}[H_2] + k_2[H] + k_3)k_{-4}k_5 + k_4k_5[C_2H_2]} \qquad (2)$$

where m_c is the mass of a carbon atom, χ is a surface density of C_{soot}-H sites ($\approx 2.3\times10^{15}$ cm^{-2}, according to Frenklach and Wang [5]) and A is the surface area. Rate constants used in this expression are listed in Table II.

Predictions of Specific Surface Growth Rates

Specific surface growth rates, R_g, were calculated according to

$$R_g = \frac{dm/dt}{A} \tag{3}$$

for each of the above expressions and by using the same value (2.3×10^{15} sites/cm^2) as derived by Frenklach and Wang [5] for χ, the surface density of C_{soot}-H sites. Comparisons of surface growth rates for three separate flames are shown in Figs. 2-4. The three flames include two of the (ethylene) Harris and Weiner flames [12] at differing stoichiometries and the acetylene flame examined by Bockhorn and coworkers [15]. For the acetylene flame, the Frenklach and Wang (FW) expression was calculated with the factor $\alpha = 0.1$. Net surface growth rates are reduced from the rates in these figures by the subtraction of oxidative terms. Oxidation has a negligible effect on the Harris and Weiner flames but affects the Bockhorn flame dramatically. The effect of oxidation will be discussed in more detail in the sensitivity section.

Figure 2 Soot growth rate constant, ethylene flame, C/O=0.96

Figure 3 Soot growth rate constant, ethylene flame, C/O=0.8

Figure 4 Soot growth rate constant, acetylene flame

Harris and Weiner measured soot growth rates for a variety of flames ($0.76\leq C/O\leq0.94$), and these data are included for comparison in Figs. 2 and 3. No data were presented for the C/O=0.96 flame, but we assume such data would lie slightly above the highest set of experimental data. Although the experimental data nearly collapses to a single curve, there is a noticeable stoichiometric dependence with the soot growth rates in the richer flames about a factor of two above those for the C/O=0.80 flame (except high in the post-flame zone where the data converge fairly well). The predicted curves tend to peak early and are all concave upwards, whereas the experimental data is concave downwards. The shape of these 'theoretical' curves is at least partially due to their dependence on H-atom concentrations and partially due to the decay in temperature. For the richer flames, all of the calculated soot growth rates predict the initial magnitude of the soot growth rate fairly well, although they all fall off too rapidly with increasing height above the burner. Furthermore, none of the models adequately describes the fall-off observed for 'older' soot particles. Consequently, we favor proposals which attribute decreasing soot growth rates with the particle ageing process. For the C/O=0.8 flame, the FW expression does not decrease by a factor of two from that for the C/O=.96 flame (in fact the FW predictions for the two flames are nearly identical) as the experimental data indicates and leads to substantial overprediction of soot formation in this leaner flame. The failure in the mechanism is due to a low dependency on the acetylene concentration. The alternative mechanisms provide a slightly better description of the stoichiometric differences between flames. In fairness to the FW mechanism, the reader should be reminded that the rate constants used in the alternative mechanisms were 'fitted' in order to obtain the agreement.

Although relative stoichiometric dependences can be described, it is also obvious that none of the models predicts the absolute magnitude of the soot growth rate data. Yet, despite the low predicted values of soot growth rates, reasonable agreement between the experimental soot profiles and the modeling of soot production is obtained. The use of benzene production as a surrogate for the inception rate undoubtedly overstates the inception process. As a result, our present model favors the use of lower surface growth rates. In general, however, we do not feel that our model is far wrong because of its reasonable agreement with the results of Frenklach and Wang, who used a more elaborate scheme for simulating the inception process. In addition, uncertainties in χ as well as the rate constants, indicates that the predicted curves in Figs. 2-4 could easily shift up or down as much as a factor of two. We have not made such shifts in the present study since uncertainties still exist in the understanding of the inception process and since the fall-off in soot growth rates

in the post-flame zone is not modeled by any of the mechanisms examined in this study. Without this fall-off, significant growth late in the post-flame zone would be predicted by our code (using any of the mechanisms described herein) if all curves were shifted upwards.

As a result of these issues, we believe that it is not the absolute magnitude that is of concern when comparing these different mechanisms, but rather the shape of the soot growth profiles within a given flame as well as the comparison of the mechanisms for several different flames.

Oxidation Processes

The per particle net rate of growth due to surface mass addition and oxidation is assumed, as discussed, to be proportional to particle surface area (free molecule form)

$$\frac{dm}{dt} = G'(t)A = G(t)m^{2/3} \quad \text{eqno(4)}$$

where A is the particle surface area, and the specific growth rate has the overall form

$$\begin{aligned} G'(t) = &(\text{Growth rate by acetylene or other growth species addition} \\ &- \text{oxidation rate by } O_2,\ OH)/\text{unit surface area.} \end{aligned} \quad (5)$$

$$\text{or} \quad G'(t) = R_G - R_{O_2} - R_{OH}$$

The mass addition term R_G in Eqns. (3) and (5) has been derived for several kinetic models of the surface growth process, as discussed in the preceding section. Oxidation of soot by OH radicals is assumed to proceed at a gas kinetic collision frequency multiplied by a collision probability of 0.13 [14]. Thus, with N_{OH}, N_A, and m_{OH} representing the OH number density, Avogadro's number, and the OH radical mass, respectively, the OH oxidation is

$$\begin{aligned} R_{OH} &= (0.13) \times N_{OH} \sqrt{\frac{KT}{2\pi m_{OH}}} \times \frac{12}{N_A} \\ &= 16.7 \frac{P_{OH}}{\sqrt{T}} \end{aligned} \quad (6)$$

where P_{OH} is the OH partial pressure in atmospheres, and the specific growth rate is in c.g.s. units. For oxidation by O_2, the Nagle & Strickland-Constable [13] expression is used.

Soot Spheroid Growth Model

The growth of soot spheroids has been modeled as an aerosol dynamics problem, involving the division of the size range of interest into discrete intervals or classes, and then solving a master equation for the size class mass densities with terms representing inception, surface growth (or oxidation), and coagulation (coalescence). The spheroids are assumed to be comprised of the single component carbon only. The sectional analysis is discussed by Gelbard and Seinfeld [25] and Gelbard, Tambour, and Seinfeld [26], and the computer program we have developed is an outgrowth of the well-known MAEROS program [8]. Because our application is specialized to the free molecule regime, we were able to simplify the calculation of growth and coagulation coefficients. The fundamental growth equations and numerical analysis algorithms are those of MAEROS, however. Soot spheroids vary in diameter from approximately one to 100 nanometers, representing a variation of six orders of magnitude in mass. In the sectional analysis, it is assumed that the boundaries of the sections vary

linearly on a log scale. The important features of the aerosol dynamics analysis are discussed by Colket and Hall [9].

Comparisons to Experimental Data

To compare theory with the soot growth data of Harris and Weiner [12] and Bockhorn, et al. [15], profiles of temperature, benzene and acetylene concentrations, and net surface growth rate are provided to the aerosol code as a function of time or height above the burner surface. The net surface growth rate consists of the mass addition rate for acetylene vapor deposition, minus oxidative terms due to oxygen molecules and OH radicals. The latter typically are dominant low in the flame, and the starting procedure for the aerosol growth analysis is to advance in time or height to the point where the net growth rate first turns positive. As will be seen, the assumptions about the inception rate and the starting procedure yield predicted onsets of growth that agree reasonably well with experimental data in most cases. The aerosol code has provision for depletion of the acetylene vapor due to deposition, but this is typically on the order of 10%, and thus does not have a major influence on the results. Certain other assumptions have been made: a size class-independent coalescence sticking probability of 1.5 is assumed, and particles with masses below 150 a.m.u. have been excluded from coalescence. As will be seen, the volume fraction tends to converge in relatively few sections, but the average particle diameter tends to require many more, so that the nominal number of sections assumed in the calculations was 25. The sensitivity of the calculations to assumptions such as these will be discussed later. Unless stated otherwise, all calculations to follow will employ the foregoing assumptions.

For comparison with the Harris flames, CHEMKIN simulations were carried out for C/O ratios of 0.8, 0.92, and 0.96 since temperature profiles were available for these flames. Experimental volume fraction data were available at values of 0.8, 0.84, 0.90, and 0.94. The comparisons of the Harris and Weiner (HW), Frenklach and Wang (FW), and modified Frenklach and Wang (MODFW) surface growth models with the data are shown in Figs. 5-7. With the exception of the Frenklach-Wang model, it can be seen that the stoichiometric dependence of the soot volume fraction is approximately satisfied. The FW model has little or no dependence on acetylene pressure (under the Harris and Weiner flame conditions), and cannot therefore reproduce the relative stoichiometric dependence with this inception model. It seems unlikely that the observed stoichiometric dependence of the volume fraction could be explained on the basis of inception alone, without a surface growth rate more strongly dependent on the acetylene concentration. The other surface growth models are seen to be reasonably consistent with the data. The FW growth model slightly overpredicts the data which is inconsistent with the presentation by Frenklach and Wang [5]. This difference is due in part to the lower benzene profile (lower by about a factor of two) which were calculated by Frenklach and Wang [5]. All the model calculations tend to suffer from overshoot at early times, particularly in the C/O=0.8 case. Suppression of coagulation involving the smallest particulates tends to raise the particle surface area. Figure 8 shows a simulation using the HW model in which all size classes are allowed to coalesce with unit sticking probability. This combination represents the best overall agreement obtained thus far, although allowing the smallest particles to undergo coalescence might well be dubious.

Figure 5 Calculated soot volume fraction, Harris flames, HW surface growth

Figure 6 Calculated soot volume fraction, Harris flames, FW surface growth

Figure 7 Calculated soot volume fraction, Harris flames, MODFW surface growth

Figure 8 Calculated soot volume fraction, Harris flames, HW surface growth

Comparison of theory and experiment for the Bockhorn flame is shown in Fig. 9. Use of the HW

rate with the 31.8 kcal activation energy gives poor agreement, serving as an indication of how uncertain the high temperature surface growth rates are. In fact, there is no reason to expect that surface growth rates can be extrapolated to the temperatures of the acetylene flame since available experimental data for specific soot growth rates is limited typically to below 1700K. Other models give more satisfactory agreement, as seen, with the MODFW model and the FW model (the latter with a 0.1 steric factor) giving the best overall agreement. If one accepts the use of this steric factor at high temperatures, the HW expression, which already gives excellent agreement with the Harris and Weiner soot data, also then describes the acetylene data very well. This good agreement is not surprising considering that the HW specific surface growth rates (see Fig. 4) are similar in shape but a factor of 10 above the sterically corrected FW rates for the acetylene flame. It is interesting to note that the simple FW expression as modified with a steric factor provides as good agreement or better as any of the more complex mechanisms - and only acetylene, benzene, and temperature profiles are required.

Figure 9 Calculated soot volume fraction, Bockhorn acetylene flame, various growth models

There is experimental evidence [27, 28, 29] and theoretical argument involving the surface density of "active sites" [24, 30, 31] that the soot growth law is of the form

$$\frac{df_v}{dt} \propto f_v - f_v^* \tag{7}$$

where f_v^* is an equilibrium, asymptotic value. A consequence of this is that a plot of rate of change of volume fraction versus volume fraction should be linear. A surface growth law proportional to total soot surface area can be consistent with (7) if the total surface area is constant and the surface reactivity has a simple exponential decay [24] therefore, we tested our simulations by making such plots from the best theory-experiment comparisons (see [9]). For the Harris 0.96 case, there is certainly a region of such linearity at the longer times where most of the experimental data exist, but in the 0.8 case it is hard to identify any such linear region. Similarly, the acetylene simulation seems somewhat ambiguous (Fig. 10), but the region of rapid growth between volume fractions of 10^{-8} and 2×10^{-8} could be said to conform to this law. Our results are not totally inconsistent with the growth law, (7), but do not yet confirm it, either. Even the experimental data [29] seems to have only a limited regime over which (7) is valid. In any case, Fig. 10 indicates that the MODFW mechanism is at least as good as the FW mechanism in providing linear plots.

Figure 10 DFVDT vs. FV, Bockhorn acetylene case

Sensitivity Studies

Size class -

The sensitivity of the C/O = 0.96 case (ethylene) to the number of size classes is exhibited in Fig. 11. The number of classes is being varied, and we specify a mass threshold (m_{min}) such that particles of mass less than this value cannot coagulate. As seen, the volume fraction tends to converge quite rapidly, with 3-5 sections giving a good approximation; the surface area has similar convergence properties. The value of volume fraction with 40 size classes differs by no more than one per cent from the value obtained with 5 classes. The optical diameter converges more slowly, requiring 25-30 sections.

Figure 11 Convergence properties of soot parameters, C/O=.96 flame, HW growth rate

Sticking probability -

Some uncertainty is associated with the proper value of the sticking coefficient, and the sensitivity of the theoretical predictions is given in Figs. 12 and 13. Lowering the sticking probability below unity

increases the surface area and contributes to much more predicted soot growth for the Harris 0.96 case. For the Bockhorn acetylene flame, however, the sensitivity is less, because the surface growth rate is relatively small except for a limited region low in the flame. The sensitivity of predicted soot volume fraction to coalescence sticking probabilities is tied to the magnitude of the local surface growth rates. Particle number densities and sizes can be expected to be much more sensitive.

Figure 12 Sensitivity to sticking probability, Harris C/O=.96, HW growth rate

Figure 13 Sensitivity to sticking probability, Bockhorn acetylene flame, MODFW growth rate

Inception rate –

If the inception or nucleation source rate is multiplied by constant factors, some impression of the sensitivity of our predictions to source rate can be gained, as shown in Fig. 14. Very significant changes are predicted for the acetylene flame when the inception rate is increased or decreased by a factor of ten. A large increase in the inception rate over the base value (m_{min} = 72 a.m.u.) is unphysical, however. Similar results were obtained for the Harris and Weiner flames, although the predictions were slightly less sensitive to decreases in the inception rate. The large sensitivity to inception rate is consistent with early models of soot formation but differs dramatically from recent suggestions. Kennedy, et al., [2] argued that as soot concentrations in flames increase, the dependence on soot inception decreases and the quantity of soot produced is dominated by growth processes. The recent experiments by Kent and Honnery [32] support these arguments. The opposing result from our model under selected conditions, we believe, is due to the fact that as inception rates decrease, the losses in surface area due to coalescence are less effective, and relatively high soot growth rates result. These opposing trends highlight the complexity of the soot formation process and the fact that conclusions drawn from one study may not be necessarily applicable to another set of conditions.

Figure 14 Predicted sensitivity to source rate, Bockhorn acetylene flames, MODFW surface growth

Minimum size for coalescing spheres –

Figure 15 displays for the Harris and Weiner 0.96 case the predicted sensitivity to the upper mass limit of small particles excluded from coalescence. This limit is the effective inception species mass in our model. The curves correspond to excluded masses of approximately 72, 150, 300, and 600 a.m.u. respectively. As seen, the sensitivity is significant. In future efforts, we hope to include the recent results of Miller [33] regarding size dependent sticking rates for polyaromatic hydrocarbons. In the previous calculations, coalescence was found only to be important for particles whose mass exceeds 800 a.m.u., much larger than those assumed to coalesce in the present study. As stated previously, identification of a more realistic (lower) inception rate will enable the model to address more reasonable descriptions of the coalescence processes.

Figure 15 Sensitivity to coagulation exclusion, Harris C/O=.96, HW growth rate

Temperature –

The importance of temperature to the soot formation process is well established [34]. The effect of temperature on benzene profiles (which in turn affects inception rates) has been shown to be significant in the report by Colket and Hall [9]. Subsequent changes in inception rates lead to nearly linear changes in soot production for most of the flames examined here. Other species, particularly H-atoms which may affect specific surface growth rates, are also a strong function of temperature. In addition, temperature may affect rate constants used in the calculation of specific surface growth rates. To examine a portion of this complex dependence on temperature, we considered the effect of uncertainties in the temperature profile on predictions using just the HW mechanism, since this

mechanism only depends on acetylene concentrations, which are weak functions of temperature. For the low pressure acetylene flames, and assuming a steric factor of 0.1 as well as the inception rates used for the base temperature case, soot profiles were calculated with temperature profiles shifted 100K above and 100K below the experimental values. These shifts resulted in about a 40% shift in the specific growth rates as well as a 30 to 50% shift in soot production. The changes in soot production due to shifts in temperature are shown in Fig. 16. Accompanying shifts in benzene profiles can be expected to enhance these differences.

Figure 16 Predicted temperature sensitivity of soot growth, acetylene flame, HW growth rate with steric factor=0.1

Oxidation –

Oxidation plays an important role because of its competition with growth processes. As described previously, soot growth calculations are initiated at the point at which growth first begins to dominate over oxidation. The relative importance of oxygen and hydroxyl radicals changes as flame conditions are altered. For the lower temperature, atmospheric pressure flames of Harris and Weiner, oxygen is the dominant oxidizer. For the higher temperature, low pressure flames of Bockhorn, et al., hydroxyl radical concentrations are much higher and OH becomes the dominant oxidizer as molecular oxygen is depleted in the flames. To examine the sensitivity of soot formation to uncertainties in the calculated OH-radical profile, we doubled the OH concentration. A substantial shift (about 5 mm) was observed in the onset of soot formation, although the total volume fraction rapidly approached the soot profile without the OH modification. These results suggest that uncertainties in OH and oxygen concentrations and/or in rate constants and processes describing the oxidation lead to uncertainties in the point of soot onset and perhaps in the early growth rates, but they do not dramatically alter total soot production. Consideration of O_2 and OH profiles relative to these issues can provide some further insight for the effect of oxidation. Oxygen is depleted dramatically in the flame front as the oxygen is consumed by the fuel. Because its precipitous drop, uncertainties in this profile and in rates of oxidation by O_2 probably have a small effect on the location of soot onset. Therefore, lower temperatures, high pressures will be less sensitive to uncertainties in oxidation processes. Hydroxyl radicals, however, peak within the flame front and slowly decay downstream as the flame cools and the radical concentrations relax to equilibrium conditions. Since this profile is so gradual, uncertainties in absolute concentrations and in rates and mechanisms can lead to substantial errors in predicting the onset of soot formation. The difficulties in accurately predicting the soot profiles for the propane flame could in part be due to uncertainties in predicting the hydroxyl radical concentrations. This analysis indicates that at elevated temperatures and low pressures, when hydroxyl radical concentrations are large, soot predictions may be quite sensitive to uncertainties in oxidation processes.

Conclusions

An analytical model of soot formation in laminar, premixed flames has been presented which is based on coupling the output of flame chemical kinetics simulations with a sectional aerosol dynamics algorithm for spheroid growth. A provisional particle inception model based on benzene formation rates is employed. Justification for the use of this simplified model is provided and its use is motivated by a desire to develop a simple procedure which might be useful for predictions in more practical flames. Surface growth has been based on experimental measurements and ab initio calculations using various possible mechanisms for the surface chemistry. In the latter, the surface growth rate becomes a function of the local values of certain gas phase species concentrations and the gas temperature. Detailed comparisons have been made with various flame data by using experimental temperature profiles and calculating profiles of species concentrations needed for the

inception rate and surface growth/oxidation calculations. Most of the models appear to overestimate soot production high in the flames. This overestimation is undoubtedly due to the fact that none of the mechanisms include effects due to particle ageing. Recent suggestions that decay of H-atoms is the cause of this 'ageing', although plausible, are inadequate because of differences between the spatial (or temporal) dependence of the decay in the H-atom profiles and the fall-off in specific growth rates observed in laboratory flames. Among the various models for the soot surface growth, best overall agreement is obtained with a modified form of the approach taken by Frenklach and Wang. The result is an analysis that is highly efficient; accurate soot volume fraction calculations can be obtained with only a few growth equations. While various aspects of this simple model can be challenged, it yields agreement with experiment that is comparable to that obtained using more elaborate models.

The modified Frenklach and Wang mechanism avoided the assumption of a high temperature steric factor, yet reproduced growth profiles while nearly providing a linear df_v/dt vs. f_v relationship. The FW mechanism was found to be deficient in that it does not properly describe the stoichiometric dependence observed in the Harris and Weiner flames; while the very simple HW expression could describe these flames as well as the acetylene flames (when the high temperature steric factor is used). Sensitivity analyses have been performed for parameters such as temperature, oxidation, number of size classes, sticking coefficients, inception rates, and coalescence of low molecular weight polyaromatic hydrocarbons. Each of these can have a significant effect on predictions of soot concentration depending on specific flame conditions.

Acknowledgements

This work has been sponsored in part by the Air Force Office of Scientific Research (AFSC), under Contracts No. F49620-88-C-0051 and F49620-85-C-0012. The United States Government is authorized to reproduce and distribute reprints for governmental purposes notwithstanding any copyright notation hereon. The authors are indebted to Dr. Julian Tishkoff, AFOSR contract monitor, for his support. The authors would like to express their appreciation to F. Gelbard for his advice and assistance on matters concerning the aerosol dynamics analysis. In addition, we would like to thank H. Bockhorn, M. Frenklach, I. Glassman, S. Harris, J. Howard, I. Kennedy, and R. Santoro for many fruitful discussions as well as for their contributions to the literature which helped to guide this research. The able assistance of K. Wicks and H. Hollick in the preparation of the manuscript and figures is gratefully acknowledged.

REFERENCES

1. S. Bhattacharjee and W. L. Grosshandler, "Effect of Radiative Heat Transfer on Combustion Chamber Flows", presented at Western States Sectional Meeting of Combustion Institute, Salt Lake City, March, (1988).
2. I. M. Kennedy, W. Kollmann, and J. Y. Chen, *Comb. and Flame,* 81:73-85, (1990).
3. R. J. Hall and P. A. Bonczyk, "Sooting Flame Thermometry Using Emission/Absorption Tomography", to appear in *Applied Optics,* (1991).
4. M.D. Smooke, P. Lin, J. K. Lam, and M. B. Long, *Twenty-Third Symposium (International) on Combustion,* The Combustion Institute, p. 575, (1990).
5. M. Frenklach and H. Wang, *Twenty-third Symposium (International) on Combustion,* The Combustion Institute, p. 1559, July, (1990).
6. J. T. McKinnon, PhD. Dissertation, Massachusetts Institute of Technology, (1989).
7. J. T. McKinnon and J. B. Howard, *Combust. Sci. Tech.,* 74:175-197, (1990).
8. F. Gelbard, *MAEROS User Manual,* NUREG/CR-1391, (SAND80-0822), (1982).
9. M.B. Colket and R.J. Hall, "Description and Discussion of a Detailed Model for Soot Formation in Laminar, Premixed Flames", United Technologies Report No. UTRC91-20, August 9, 1991. Also Appendix A in M. B. Colket, R. J. Hall, J. J. Sangiovanni, and D. J. Seery, "The Determination of Rate-Limiting Steps During Soot Formation", Final Report to AFOSR, under Contract No. F49620-88-C-0051, UTRC Report no. 91-21, August 14, (1991).
10. R. J. Kee, J. F. Gcar, M. D. Smooke, an J. A. Miller, "A Fortran Program for Modeling Steady Laminar One-Dimensional Premixed Flames", Sandia report, SAND85-8240, (1985).
11. R. J. Kee, R. M. Rupley, and J. A. Miller, "CHEMKIN II: A Fortran Chemical Kinetics Package for the Analysis of Gas-Phase Chemical Kinetics", Sandia Report, SAND89-8009-UC-401, September, (1989).
12. S. J. Harris and A. M. Weiner, *Combust. Sci. Tech.,* 31:155-167, (1983).
13. J. Nagle and R.F. Strickland-Constable, *Proceedings of the Fifth Carbon Conference,* Vol. 1, Pergamon Press, p. 154, (1963).
14. K. G. Neoh, J. B. Howard, and A. F. Sarofim, *Particulate Carbon: Formation During Combustion,* D. C. Seigla and G. W. Smith, eds. Plenum, New York, p. 261, (1981).
15. H. Bockhorn, F. Fetting and H. W. Wenz, *Ber. Bunsenges. Phys. Chem.,* 87:1067, (1983).
16. S. J. Harris, A. M. Weiner, R. J. Blint, *Comb. and Flame,* 72:91-109, (1988).
17. J. A. Miller and C. F. Melius, "Kinetic and Thermodynamic Issues in the Formation of Aromatic Compounds in Flames of Aliphatic Fuels", to be published in *Comb. and Flame,* (1991).
18. J. A. Miller and C. T. Bowman, *Progress in Energy and Combustion Science,* 15:287-338 (1989).
19. C.K. Westbrook and F.D. Dryer, *Prog. Energy Combust. Sci.,* 10:1-57 (1984).
20. F. Communal, S. D. Thomas, and P. R. Westmoreland, "Kinetics of C3 Routes to Aromatics Formation", Poster paper (P40) presented at the Twenty-Third Symposium on Combustion, Orleans, France, July, (1990).
21. S.E. Stein, J. A. Walker, M. Suryan and A. Fahr, *Twenty-Third Symposium (International) on Combustion,* The Combustion Institute, p. 85, (1990)
22. M. Frenklach and H. Wang, "Aromatics Growth Beyond the First Ring and the Nucleation of Soot Particles", presented at the 202nd American Chemical Society, National Meeting, New York, August 25-30, 1991, also *Division of Fuel Chemistry Reprints,* 36(4):1509-1516, (1991).

23. R. D. Kern, C. H. Wu, J. N. Yong, K. M. Pamidimukkala, and H. J. Singh, "The Correlation of Benzene Production with Soot Yield Determined from Fuel Pyrolysis", presented at the American Chemical Society, National Meeting, Division of Fuel Chemistry, New Orleans, Fall, (1987).
24. C. J. Dasch, Comb. Flame 61:219-225, 1985.
25. F. Gelbard and J. H. Seinfeld, *J. Coll. Int. Sci.*, 78:485-501, (1980).
26. F. Gelbard, Y. Tambour, J. H. Seinfeld, *J. Coll. Int. Sci.*, 76:54-556, (1980).
27. B. S. Haynes and H. G. Wagner, Z. Physikalishe Chemie NF, 133:201, 1982.
28. U. Wieschnowsky, H. Bockhorn, and F. Fetting, Twenty-Second Symposium (International) on Combustion, The Combustion Institute, p. 343, 1988.
29. H. Bockhorn, F. Fetting, A. Heddrich, and G. Wannemacher, *Twentieth Symposium (International) on Combustion,* The Combustion Institute, p. 979, (1984).
30. S. J. Harris, Combust. Sci. Tech., 72:67-77, 1990.
31. I. T. Woods and B. S. Haynes, Combustion and Flame, 85:523,1991.
32. J. H. Kent and D. R. Honnery, *Combust. Sci. Tech.*, 75:167-177, (1991).
33. J. H. Miller, *Twenty-Third Symposium (International) on Combustion,* The Combustion Institute, p. 91, (1990).
34. I. Glassman, *Twenty-Second Symposium (International) on Combustion,* The Combustion Institute, p. 295-311, (1988).

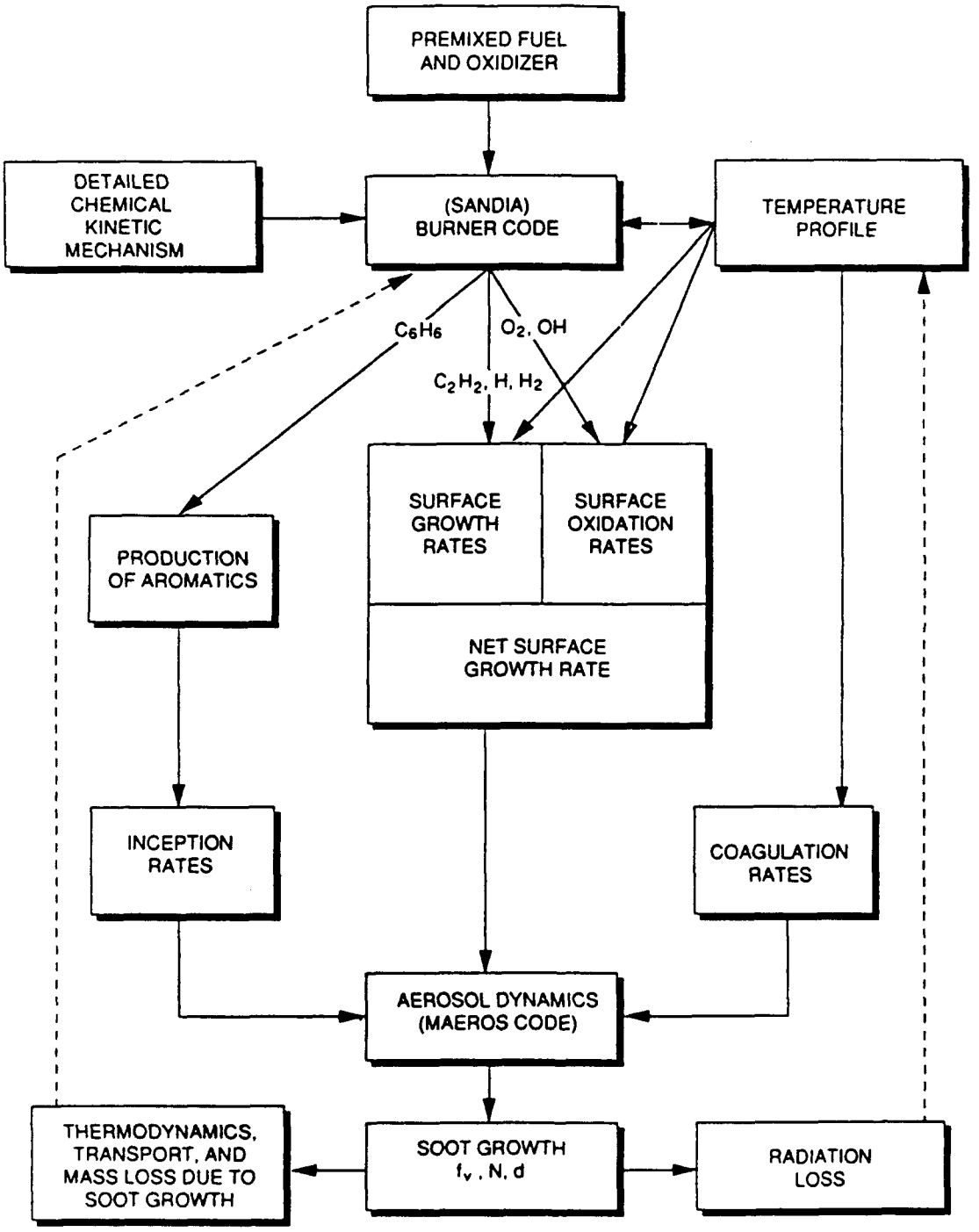
PREMIXED FUEL AND OXIDIZER
DETAILED CHEMICAL KINETIC MECHANISM
(SANDIA) BURNER CODE
TEMPERATURE PROFILE
C_6H_6
O_2, OH
C_2H_2, H, H_2
PRODUCTION OF AROMATICS
SURFACE GROWTH RATES
SURFACE OXIDATION RATES
NET SURFACE GROWTH RATE
INCEPTION RATES
COAGULATION RATES
AEROSOL DYNAMICS (MAEROS CODE)
THERMODYNAMICS, TRANSPORT, AND MASS LOSS DUE TO SOOT GROWTH
SOOT GROWTH f_v, N, d
RADIATION LOSS

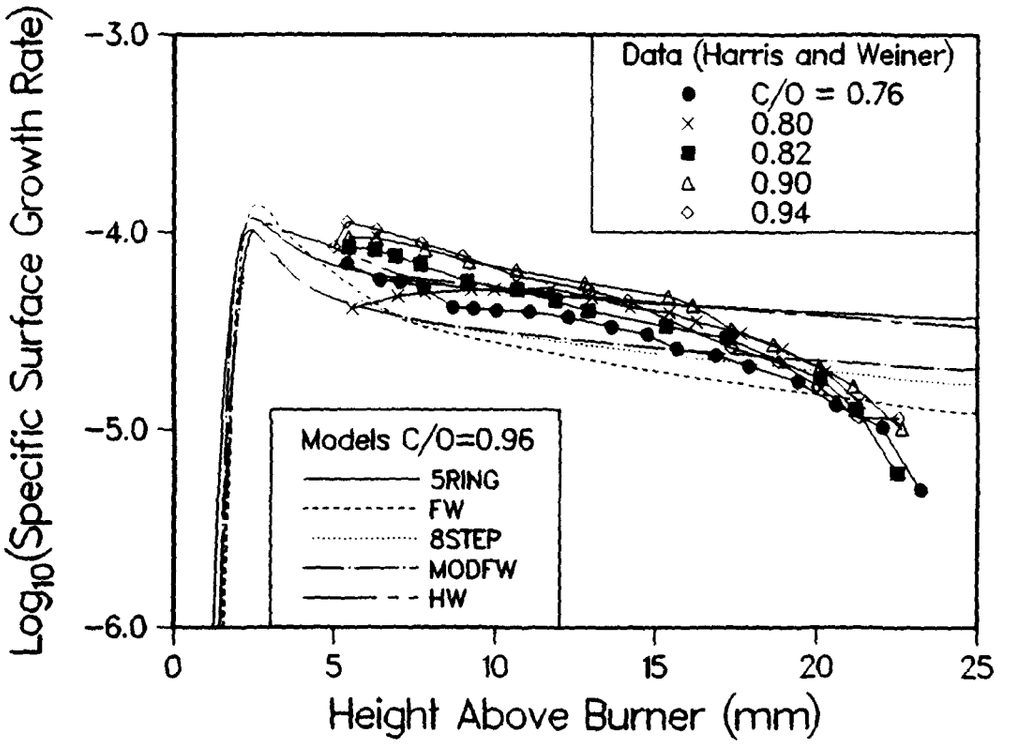
Log10(Specific Surface Growth Rate)
-3.0
-4.0
-5.0
-6.0
0
5
10
15
20
25
Height Above Burner (mm)
Data (Harris and Weiner)
C/O = 0.76
0.80
0.82
0.90
0.94
Models C/O=0.96
5RING
FW
8STEP
MODFW
HW

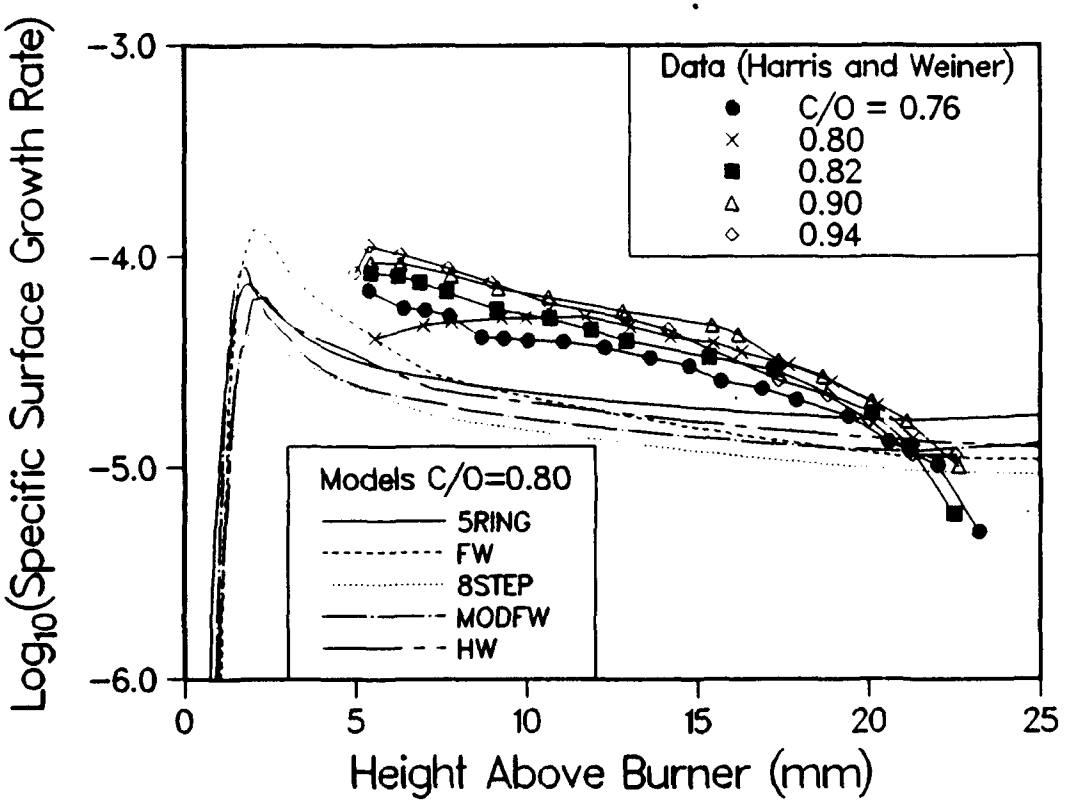
Log10(Specific Surface Growth Rate)
-3.0
-4.0
-5.0
-6.0
0
5
10
15
20
25
Height Above Burner (mm)
Data (Harris and Weiner)
C/O = 0.76
0.80
0.82
0.90
0.94
Models C/O=0.80
5RING
FW
8STEP
MODFW
HW

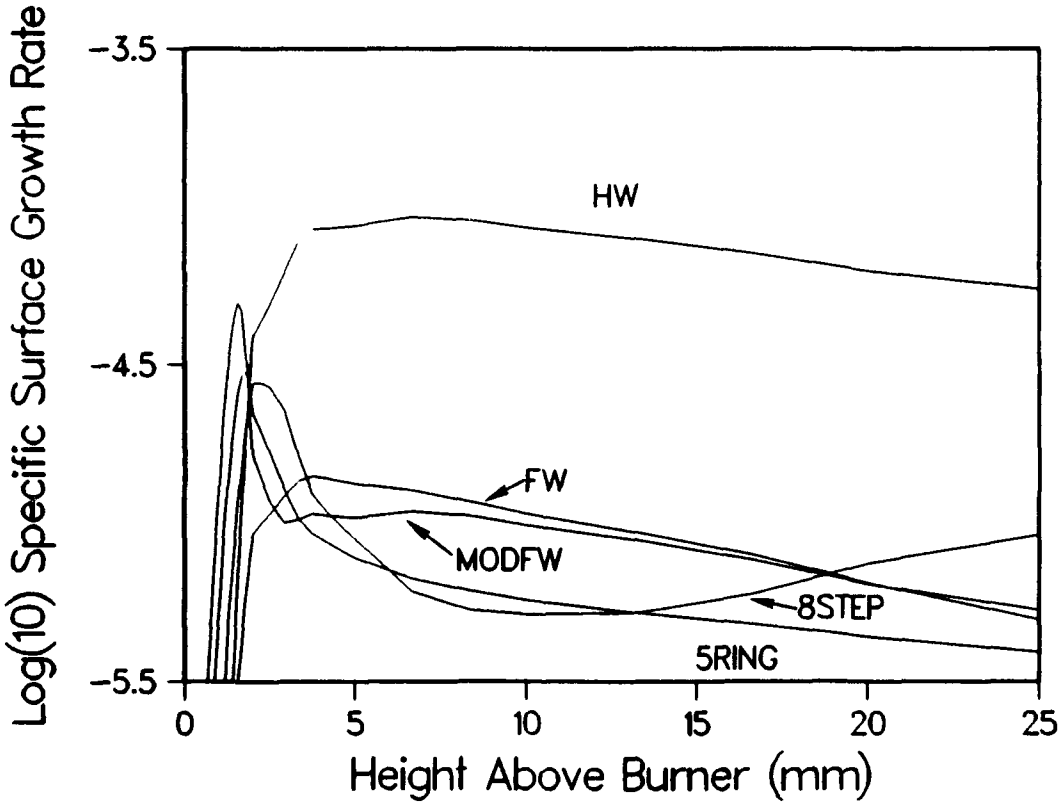
Log(10) Specific Surface Growth Rate
-3.5
-4.5
-5.5
0
5
10
15
20
25
Height Above Burner (mm)
HW
FW
MODFW
8STEP
5RING

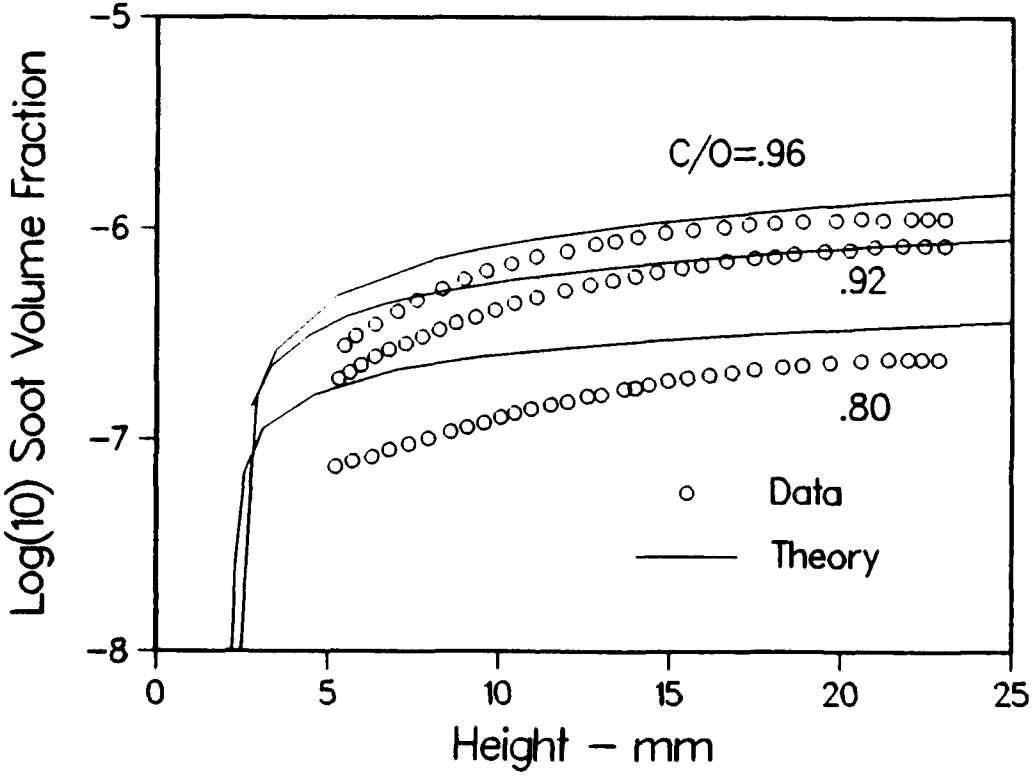
Log(10) Soot Volume Fraction
-5
-6
-7
-8
0
5
10
15
20
25
Height – mm
C/O=.96
.92
.80
Data
Theory

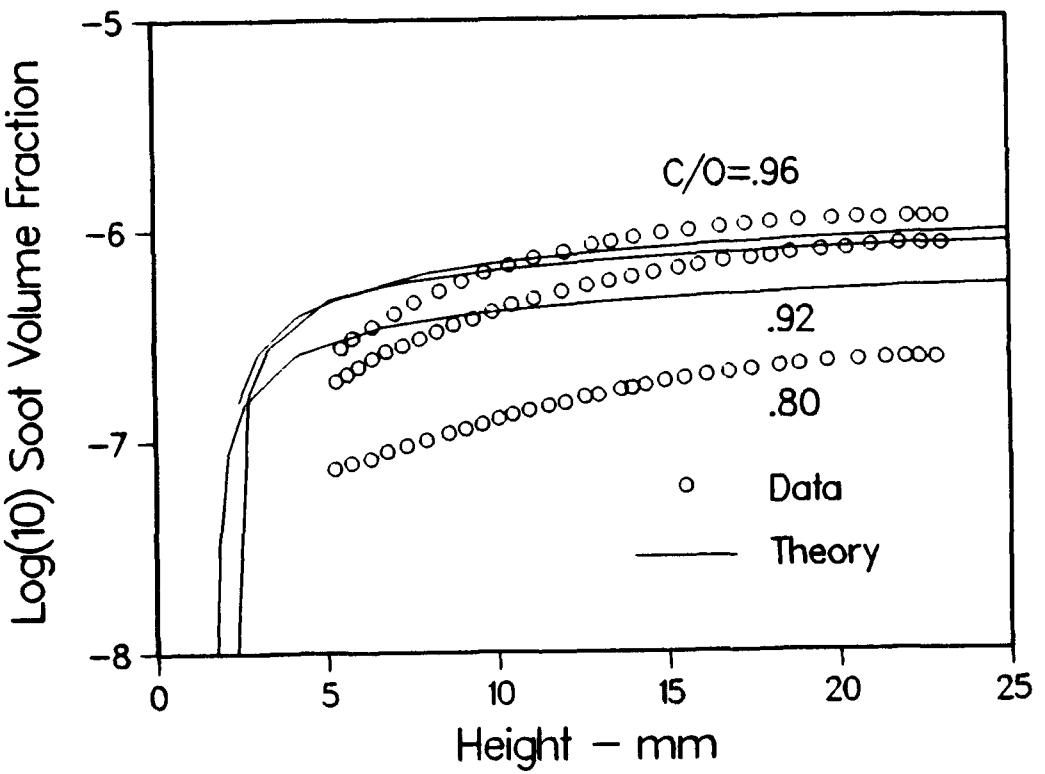
Log(10) Soot Volume Fraction
-5
-6
-7
-8
0
5
10
15
20
25
Height – mm
C/O=.96
.92
.80
Data
Theory

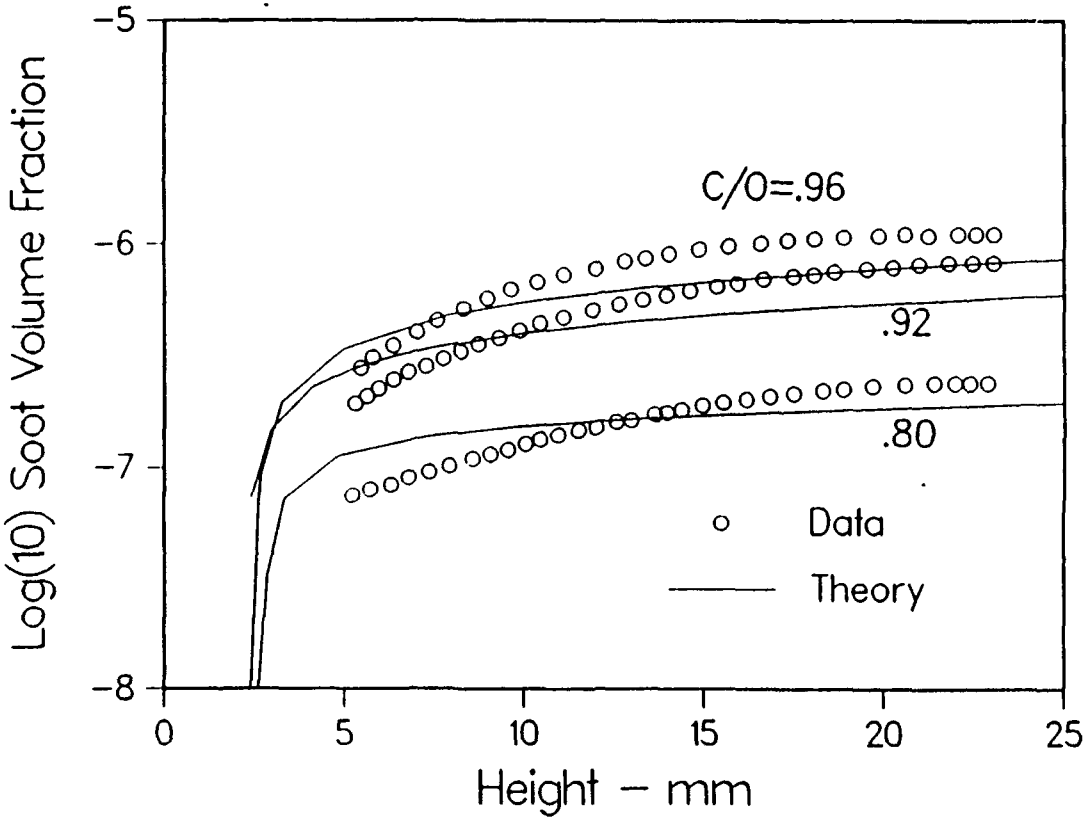
Log(10) Soot Volume Fraction
-5
-6
-7
-8
0
5
10
15
20
25
Height – mm
C/O=.96
.92
.80
Data
Theory

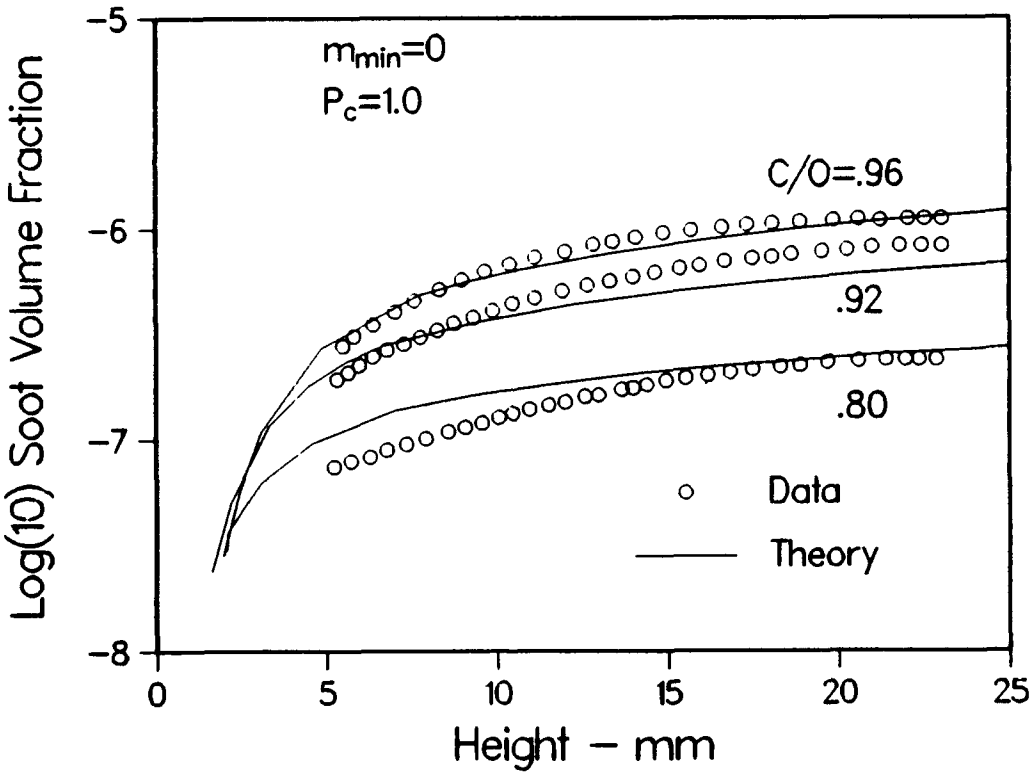
m_{min}=0
P_c=1.0
C/O=.96
.92
.80
Data
Theory
Log(10) Soot Volume Fraction
-5
-6
-7
-8
0
5
10
15
20
25
Height – mm

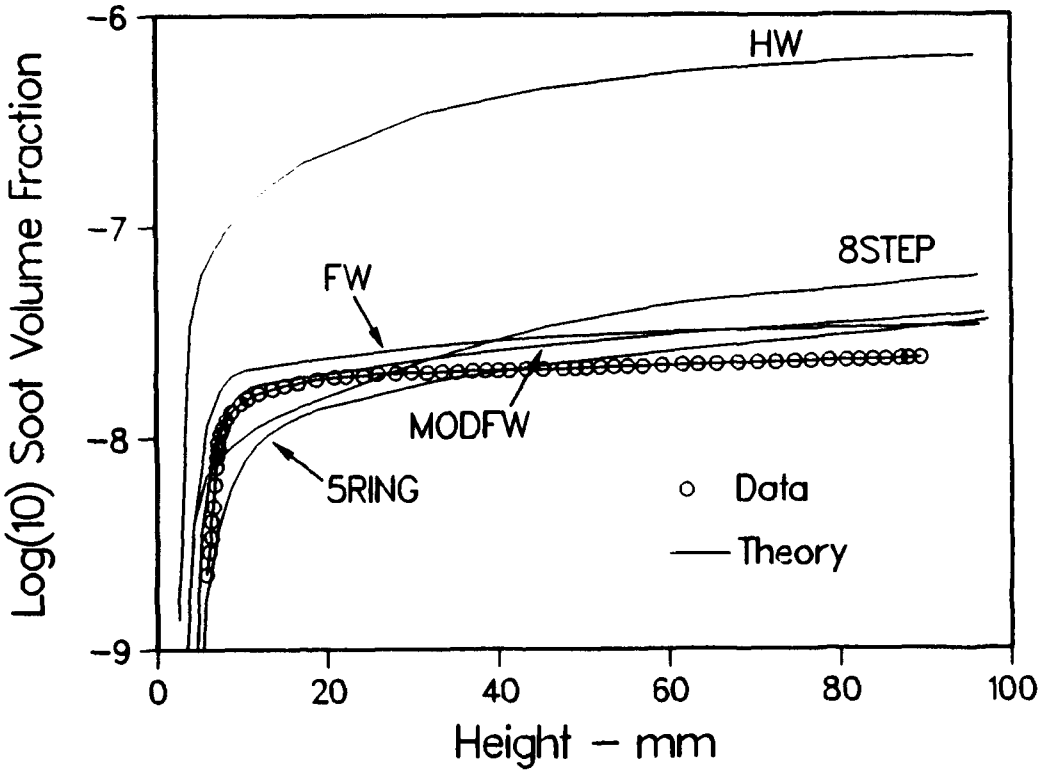
Log(10) Soot Volume Fraction
-6
-7
-8
-9
0
20
40
60
80
100
Height – mm
HW
8STEP
FW
MODFW
5RING
Data
Theory

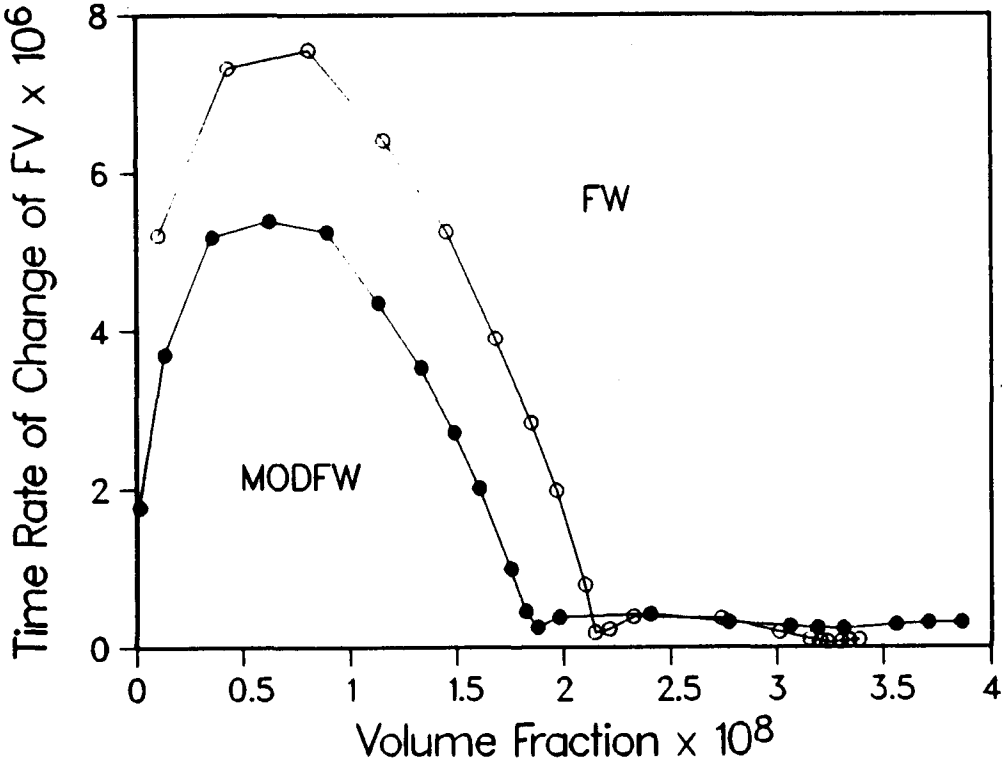
Time Rate of Change of FV x 10^6
8
6
4
2
0
FW
MODFW
0
0.5
1
1.5
2
2.5
3
3.5
4
Volume Fraction x 10^8

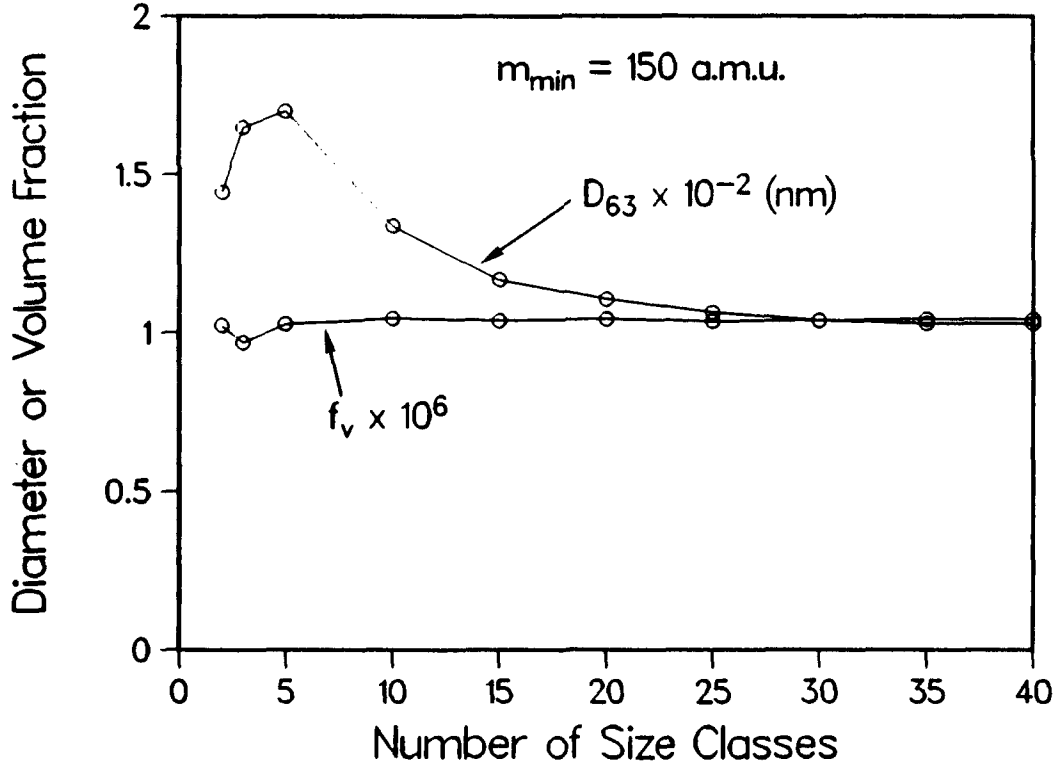
m_{min} = 150 a.m.u.
$D_{63} \times 10^{-2}$ (nm)
$f_v \times 10^6$
Diameter or Volume Fraction
Number of Size Classes
0
0.5
1
1.5
2
0
5
10
15
20
25
30
35
40

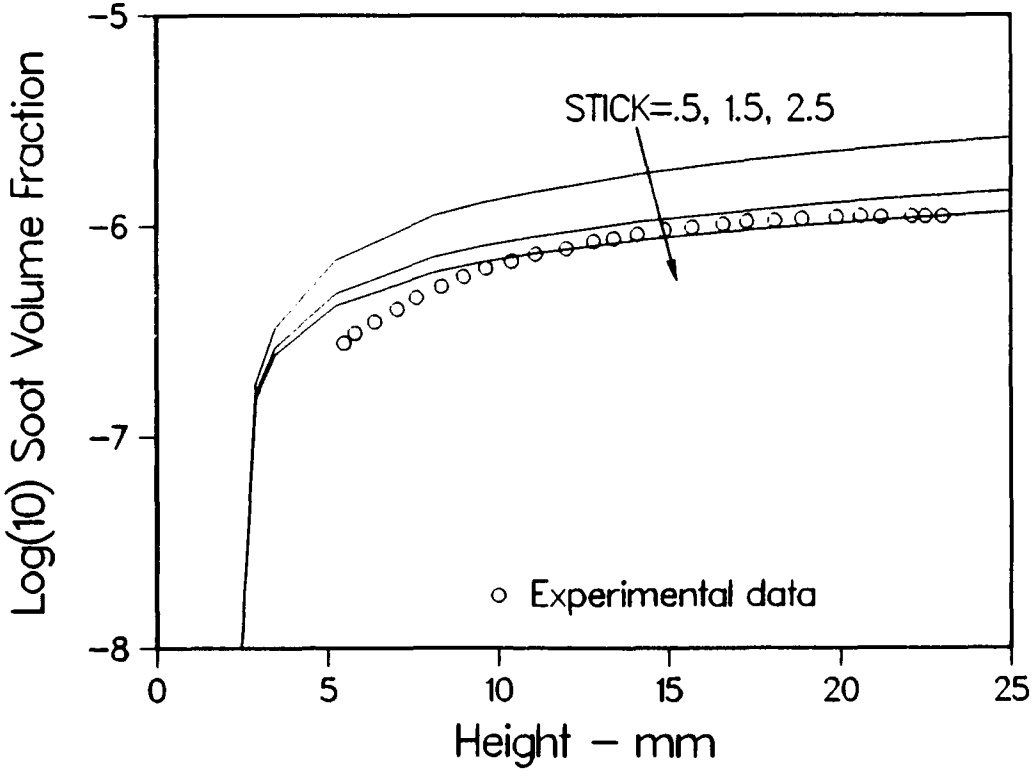
Log(10) Soot Volume Fraction
-5
-6
-7
-8
0
5
10
15
20
25
Height – mm
STICK=.5, 1.5, 2.5
o Experimental data

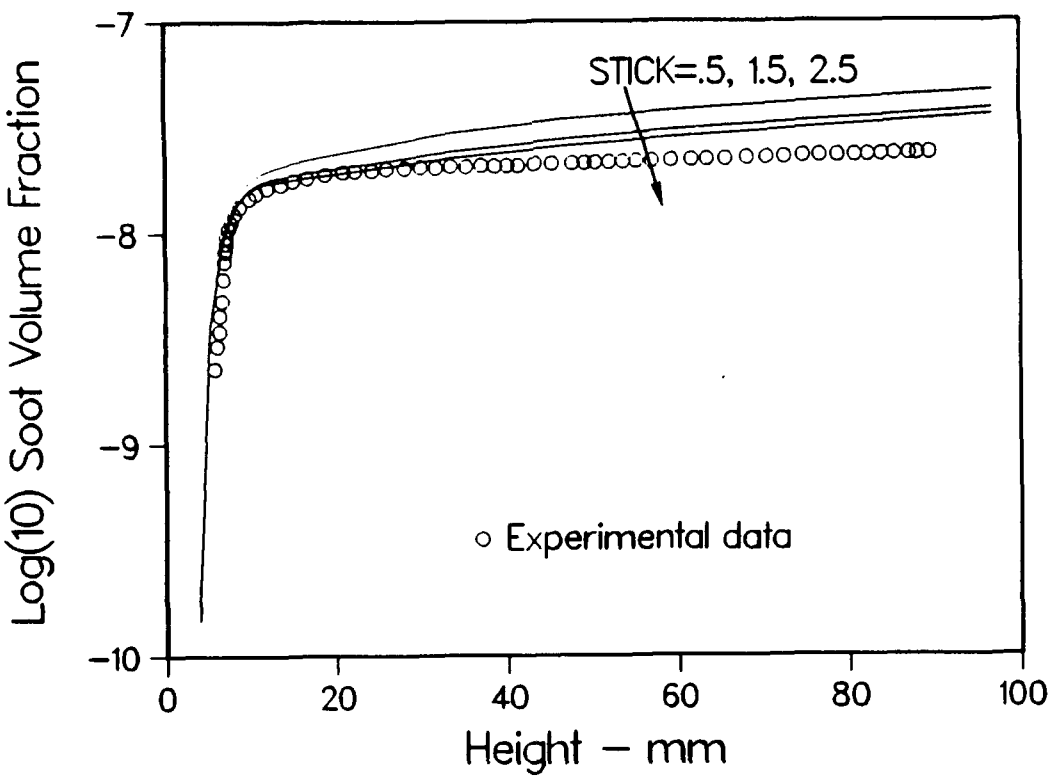
STICK=.5, 1.5, 2.5
o Experimental data
Log(10) Soot Volume Fraction
−7
−8
−9
−10
0
20
40
60
80
100
Height − mm

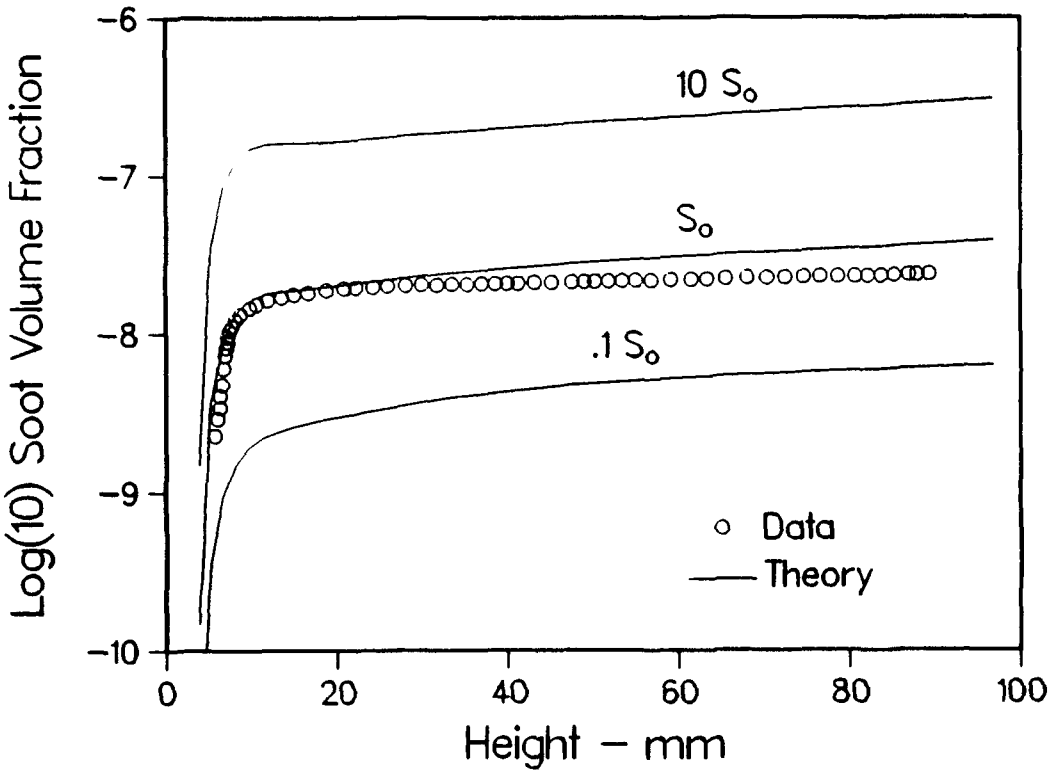
Log(10) Soot Volume Fraction
-6
-7
-8
-9
-10
0
20
40
60
80
100
Height – mm
10 S_o
S_o
.1 S_o
Data
Theory

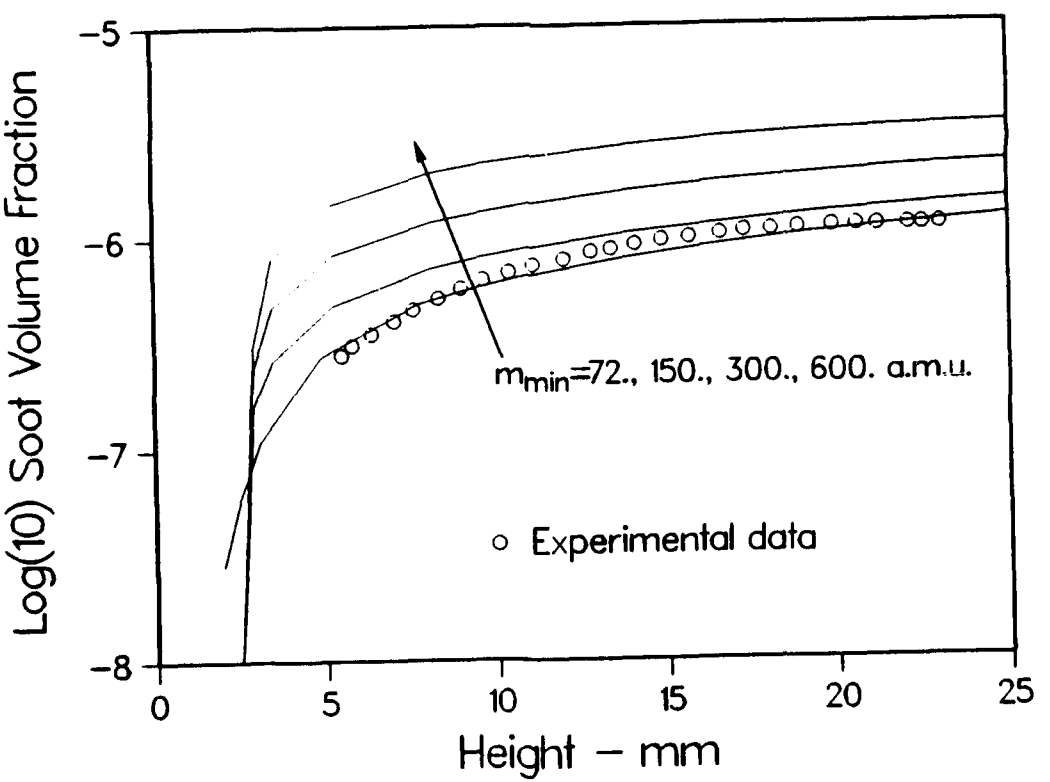
Log(10) Soot Volume Fraction
−5
−6
−7
−8
0
5
10
15
20
25
Height − mm
m_{min}=72., 150., 300., 600. a.m.u.
o Experimental data

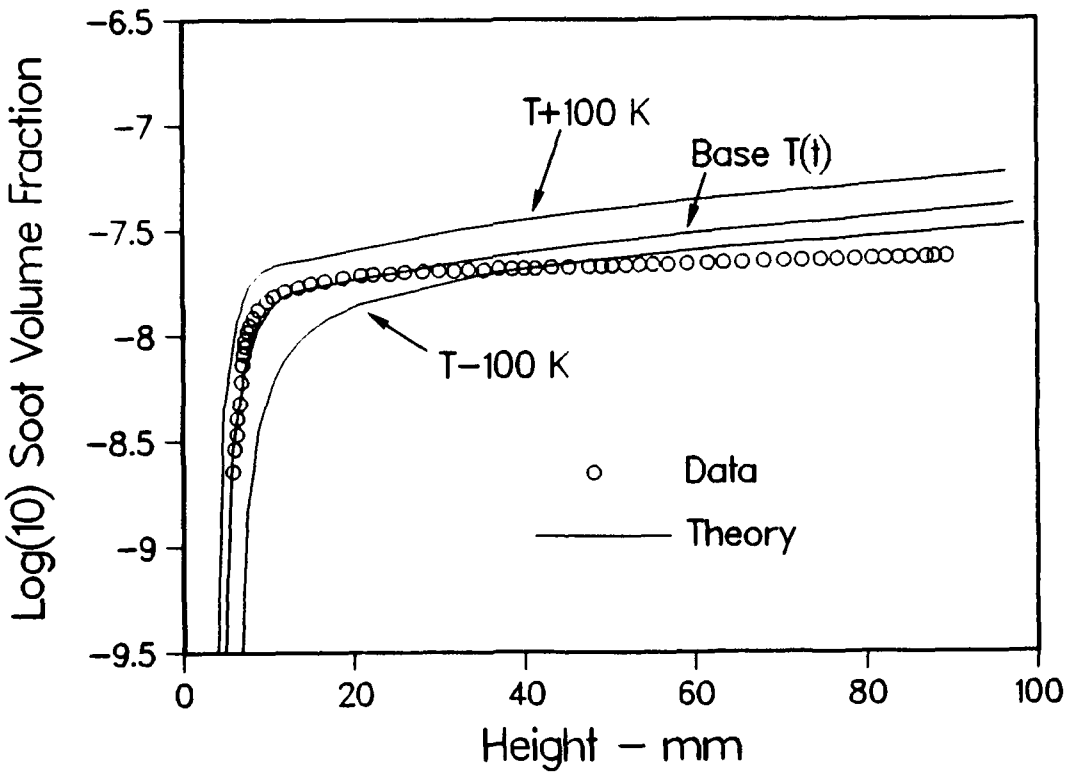
Log(10) Soot Volume Fraction
-6.5
-7
-7.5
-8
-8.5
-9
-9.5
0
20
40
60
80
100
Height – mm
T+100 K
Base T(t)
T–100 K
Data
Theory

Appendix C

The Radiative Source Term for Plane-Parallel Layers of Reacting Combustion Gases

The Radiative Source Term for Plane-Parallel Layers of Reacting Combustion Gases

by

Robert J. Hall
United Technologies Research Center
East Hartford, Conn.

An expression is derived for the radiative source term governing the interaction of molecular gas band radiation and flow in nonhomogeneous, plane-parallel reacting flow problems. The divergence of the net radiative flux is formulated in terms of wideband absorptance model parameters for combustion products, and is valid for all degrees of optical thickness. When optical thickness is finite, the net absorption is obtained by integrating the radiation field solution over the band lineshapes and taking hemispherical averages. Illustrative calculations for counterflow diffusion flames will be discussed.

Funded by AFOSR Contract F49620-91-C-0056

Introduction

A recognized effect of radiation from flames is that substantial fractions of energy can be lost from the flame environment. In addition to radiative loading of enclosure walls, this energy loss leads to a temperature reduction and therefore changes in local gas density and flow velocity as well. In extreme cases, the reduction in flame velocity can lead to a substantial reduction in flame length. In addition, the temperature reduction affects flame chemistry due to the Arrhenius-exponential dependence on temperature. Errors in temperature could lead to substantial inaccuracies in calculating formation rates of nitric oxide, for example. While all of these effects can be expected to be most extreme in sooting flames, non-luminous gas band radiation can be important, as well, and the way in which one couples the radiation and flow calculations for quantitative assessment of these effects in plane-parallel or boundary layers of combustion gas products is the subject of this paper.

Analysis

The coupling between radiation and flow occurs mathematically in the flow energy equation, and can be represented in all generality in the form

$$\frac{DH_0}{Dt} = -\frac{\partial q_i^R}{\partial x_i} \tag{1}$$

where DH_0/Dt is a generalized representation of the rate of change of total enthalpy (H_0) which can include convection, transport, and chemical enthalpy release, and $\frac{\partial q_i^R}{\partial x_i}$ is the divergence of the net radiative flux. From the equation of radiative transfer is possible to show that

$$\frac{\partial q_i^R}{\partial x_i} = \int_0^\infty d\omega \int_{4\pi} d\vec{\Omega}\, K_a(\omega)\, \left[I_b(\omega) - I(\vec{\Omega},\omega)\right] \tag{2}$$

$$I_b(\omega) = 1.1925\text{x}10^{-5}\, \omega^3/(\exp\,(1.438\,\omega/T) - 1) \qquad (\text{c.g.s.;}\,\omega \text{ in } \text{cm}^{-1})$$

where K_a is the local aborption coefficient, I_b is the local Planck body function, and I is the local radiative flux. The integrals over all frequencies and directions of radiation propagation ($\vec{\Omega}$) must be taken. In the optically thin limit, the second term can be neglected, and the isotropic source term is equivalent to

$$\left.\frac{\partial q_i^R}{\partial x_i}\right|_{EMISS} = 4\pi \int_0^\infty d\omega \; K_a(\omega) \; I_b(\omega) \tag{3}$$

Because only frequency-integrated quantities are required, with no need for calculations of spectral detail, it seems adequate to use wide-band models for the absorption bands of the species that are important in combustion product radiation (CO_2, H_2O, and CO). In the wide-band formulation the local absorption coefficient for band j belonging to species i is represented by

$$K_a(\omega) = K_{aij}(\omega) = \frac{\alpha_{ij}\rho_i}{\omega_{ij}} \exp\left(-\frac{C_0\,|\omega - \omega_{ij}^{(c)}|}{\omega_{ij}}\right) \tag{4}$$

where α_{ij} is the integrated band intensity (units: $cm^{-1}/(gm \cdot cm^{-2})$), ω_{ij} is the bandwidth; ρ_i is the mass density of optically active chemical species i; $\omega_{ij}^{(c)}$ is the band center; and C_0 = 1 or 2 depending on whether the band is one-sided or symmetric. With the assumption that I_b varies more slowly with frequency than the absorption bandshape, Equation 3 can be simply expressed as (Ref. 1):

$$\left.\frac{\partial q_i^R}{\partial x_i}\right|_{EMISS} = 4\pi \sum_{ij} \alpha_{ij} \; \rho_i \; I_{bij} \tag{5}$$

$$I_{bij} = I_b(\omega_{ij}^{(c)}, T)$$

where the summation is over all bands and species, and I_{bij} is the Planck function evaluated at the band center. Tabulations of the band model parameters for the important vibrational infrared and pure rotational transitions and the way in which one computes their temperature dependences are given in Refs. 2 & 3. We have nominally included in our model all fifteen bands listed for H_2O, CO_2, & CO. The optically thin or Planck limit expression given in Equation 5 is convenient because it depends only on local parameters, and does not depend on having an optical field solution. The coupling between radiation and flow in counterflow diffusion flames has been examined in this emission-dominated limit in Refs. 4 & 5, and it has been found that radiation can severely depress peak temperatures and have a strong influence on NO_x production for low strain rates. However, very low strain rates correspond to thicker flames where optical thickness effects could become important, and the purpose of the rest of this paper is to derive an expression for

the absorption term in Equation 2 for plane parallel layers where all medium properties vary in one coordinate only, say y:

$$\left.\frac{\partial q_y^R}{\partial y}\right|_{ABS} = -\int_0^\infty d\omega \int_{4\pi} d\vec{\Omega}\, K_q(\omega)\, I(\vec{\Omega},\omega) \tag{6}$$

The way in which this is done is to derive a solution for the frequency-dependent optical field, carry out the hemispherical average by interchanging orders of integration, and then perform the frequency integral in Equation (6). The coordinate system employed is given in Figure 1; a boundary layer problem in which medium properties vary only in the y-direction is assumed, and cold, black walls will also be assumed in the interests of simplicity. The effect of hot walls will be discussed later. It is convenient to carry out the calculation for a single band, and then sum over all bands/species at the end; a further approximation made here is to neglect band overlap effects which are usually relatively small. At a given depth y, the sum of the intensities with direction cosines μ and $-\mu$, respectively, can be formally represented by

$$\begin{aligned} I_{ij}(\mu,\omega) + I_{ij}(-\mu,\omega) = &\int_0^y I_b(y',\omega)\frac{d\tau_{ij}}{d(y'/\mu)}\frac{dy'}{\mu} \\ &+ \int_y^\infty I_b(y',\omega)\frac{-d\tau_{ij}}{d(y'/\mu)}\frac{dy'}{\mu} \end{aligned} \tag{7}$$

where τ_{ij} is the transmissivity given for wide-band models by

$$\tau_{ij} = \exp\left(\frac{-\bar{\bar{K}}_{aij}(\omega)\,|y-y'|/\mu}{\sqrt{1+\frac{\bar{\bar{K}}_{aij}(\omega)\,|y-y'|/\mu}{\bar{\beta}_{ij}\,p_{e,i}}}}\right)$$

$$\bar{\bar{K}}_{aij}(\omega) = \frac{\bar{\alpha}_{ij}\bar{p}_i}{\bar{\omega}_{ij}}\exp\left(-C_0\frac{|\omega-\omega_{ij}^{(o)}|}{\bar{\omega}_{ij}}\right) \tag{8}$$

where $\beta_{i,j}$ and $p_{e,i}$ are the equivalent line width parameter equivalent broadening pressure for the band, respectively. The band model parameters are here represented by overbars to indicate that they are equivalent homogeneous path parameters whose method of calculation will be discussed later. Modak (Ref. 6) has shown that it is a good approximation in flame calculations to assume the high broadening limit for which

$$\tau_{ij} = \exp(-\overline{K}_{aij}(\omega)\ \frac{|y - y'|}{\mu}) \tag{9}$$

This approximation should be particularly good for the high-pressure, counterflow flame calculations to be given later. In this limit, Equation (7) is

$$I(\mu,\omega) + I(-\mu,\omega) = \int_0^\infty dy'\ I_b(y',\omega)\ \overline{K}_a(\omega) \exp \left(-\overline{K}_a(\omega)\ |y - y'|/\mu\right) dy'/\mu \tag{10}$$

where the ij subscripts have temporarily been suppressed in the interests of notational simplicity.

The orientation average in Equation 6 is equivalent to the hemispherical average

$$\int_{4\pi} d\Omega\ [\text{Eq. 10}] = 2\pi \int_0^1 d\mu\ [\text{Eq. 10}] \tag{11}$$

Performing this integration and making the transformation $z = \exp\left(-C_0\ \frac{|\omega - \omega'|}{\overline{\omega}}\right)$, for the frequency integration, Eq. 6 is equal to

$$-2\pi\ \frac{\alpha\rho}{\omega} \int_0^\infty dy'\ I_b\ \overline{\alpha}\ \overline{\rho} \int_0^1 dz\ z^{(\overline{\omega}/\omega)}\ E_1\left(\frac{\overline{\alpha}\ \overline{\rho}}{\overline{\omega}}\ |y - y'|\ z\right) \tag{12}$$

where E_1 is the exponential integral and the slowly varying Planck function has been moved outside the z-integral. The z-integral is given by (Ref. 7)

$$\left[\ \gamma(1 + \overline{\omega}/\omega, u)/u^{(1+\overline{\omega}/\omega)} + E_1(u)\ \right] \tag{13}$$

where $u = \frac{\overline{\alpha}\ \overline{\rho}}{\overline{\omega}}\ |y - y'|$ is the band center optical depth and γ is the incomplete gamma function as given in Abramovitz and Stegun (Ref. 8). It is more convenient to use the γ^* form given for which (Ref. 8)

$$\gamma(1 + \overline{\omega}/\omega, u)/u^{(1+\overline{\omega}/\omega)} = \Gamma(1 + \overline{\omega}/\omega)\gamma^*(1 + \overline{\omega}/\omega, u) \tag{14}$$

The γ^* function can be efficiently calculated using the series representation of Ref. 8. Summing over all species and bands gives the final result for the net absorption of radiant energy by the medium

$$\frac{\partial q_y^R}{\partial y}\Big|_{ABS} = -2\pi \sum_{ij} \left(\frac{\alpha\rho}{\omega}(y)\right)_{ij} \int_0^\infty dy' I_{bij}(\bar{\alpha}\,\bar{\rho})_{ij} \left[\Gamma(1+\bar{\omega}/\omega)\gamma^*(1+\bar{\omega}/\omega, u) + E_1(u)\right]_{ij} (1+\bar{\omega}/\omega)_{ij}^{-1} \tag{15}$$

where $u = u_{ij} = \left(\frac{\bar{\alpha}\,\bar{\rho}}{\bar{\omega}}\right)_{ij} |y - y'|$.

The calculation of the equivalent homogeneous path band model parameters ($\bar{\alpha}, \bar{\rho}$, and $\bar{\omega}$) is based on the Curtis-Godson approximation as given by Felske and Tien (Ref. 9). The temperature and species densities are simple path averages between point y and the point y′ in the running integral; $\alpha = \alpha(\bar{T})$, and $\omega = \xi\omega(\bar{T})$, where ξ is a correction factor (Refs. 6,10) ranging from 1.0 to 1.44. The procedure for calculating ξ by bilinear interpolation based on the nominal, band-center optical depth u_{ij} and equivalent line width parameter $\beta(\bar{T})$ is given in Ref. 6,10. For the H_2O pure rotational band, the band model parameters of Ref. 11 are *nominally used; for this band*, $\xi = 1$.

An alternative form for Equation (15) is derived by converting the integration over y′ in Equation (7) to an integration over τ. If one has medium properties on a grid of points denoted by the index l, Equation (15) can be shown to be equivalent to

$$\frac{\partial q_y^R}{\partial y}\Big|_{ABS} = -2\pi \sum_{ij} \left(\frac{\alpha\rho}{\omega}(y)\right)_{ij} \sum_{\ell} \bar{\omega}_{ij}^{(\ell)}\, \bar{I}_{bij}^{(\ell)} \left(\Upsilon_{ij}(\ell_+ \to y) - \Upsilon_{ij}(\ell_- \to y)\right)$$

$$-2\pi \sum_{ij} \left(\frac{\alpha\rho}{\omega}(y)\right)_{ij} \left[\bar{\omega}_{ij}^{(1)} I_{bij}(T_{w1}) \Upsilon_{ij}(1 \to y) + \bar{\omega}_{ij}^{(2)} I_{bij}(T_{w2})\, \Upsilon_{ij}(2 \to y)\right. \tag{16}$$

where

$$\Upsilon = \Gamma(\bar{\omega}/\omega)\gamma^*(\bar{\omega}/\omega, u) - \frac{u}{1+\bar{\omega}/\omega} \left(E_1(u) + \Gamma(1+\bar{\omega}/\omega)\gamma^*(1+\bar{\omega}/\omega, u)\right)$$

and it has been assumed that all path averages are taken from point y to the grid midpoints, and that ω and I_b are evaluated at the midpoints. The functions $\Upsilon_{ij}(\ell_+ \rightarrow y)$ and $\Upsilon_{ij}(\ell_- \rightarrow y)$ are based on which of the grid point pairs is closest to and farthest from y, respectively. The effect of absorption of hot, black wall radiation has been introduced in the terms involving the wall temperatures T_{w1} and T_{w2}; it is understood that the path-averaged properties which go into $\bar{\omega}$ and Υ in these terms are those along the paths from each wall to point y.

Equations 15 and 16 can be time-consuming to use because of the running integrals that must be evaluated for each point y. The "analytic" approximation of Modak (Ref. 6) provides increased efficiency and reasonable accuracy when the radiating species are concentrated in a high temperature reaction sheet as encountered in diffusion flames. Returning to Equation 7, it is reasoned that most of the contribution to the integrals will come from regions near the maximum flame temperature because of the rapid variation of Ib with temperature. The transmissivity derivatives will be more slowly varying, and can be factored out, assigned their values at $y = y_f$, the point of maximum flame temperature. This gives, for cold, black walls:

$$\left.\frac{\partial q^R}{\partial y}\right|_{ABS} = -2\pi \sum_{ij} \left(\frac{\alpha\rho}{\omega}(y)\right)_{ij} \left[\frac{\bar{\alpha}\,\bar{\rho}}{1+\bar{\omega}/\omega}\left(\Gamma(1+\bar{\omega}/\omega)\gamma(1+\bar{\omega}/\omega, u) + E_1(u)\right)\right]_{ij} \int dy'\, I_{bij} \tag{17}$$

$$\int dy'\, I_{bij} = \int_0^y dy' I_{bij} \qquad (y > y_f)$$

$$= \int_y^\infty dy' I_{bij} \qquad (y < y_f)$$

and the property averages are calculated between y and y_f. Equation (17) gives results nearly equivalent to Equations 15 and 16 with much increased efficiency, subject to one restriction that will be discussed in the next section. Absorption of hot wall absorption can be represented by the same terms as in Equation 11. These expressions are not limited to slowly varying medium properties per se, but would presumably have the inherent limitations of the Curtis-Godson approximation in this regard.

Sample Calculated Results

Example calculations have been done for an opposed jet diffusion flame, as illustrated in Figure 1. The configuration consists of two opposed fuel and oxidizer jets, and is known (Ref. 12) to lead to a one-dimensional structure normal to the surface of stoichiometric mixture. In a small region near the stagnation streamline, temperature and species concentrations are nearly one-dimensional. Temperature and radiating species concentrations have been computed using a counterflow flame code developed by Smooke (Ref. 12). The calculations are described in more detail in Ref. 13, where they formed the basis for a flamelet approach to predicting NO_x concentrations in an aircraft gas turbine combustor. The pressure is 10.5 atm, and the fuel temperature has been chosen to give an adiabatic flame temperature approximating that of jet fuel. The temperature and radiating species profiles are shown in Figures 2 and 3 for the base case used in these calculations. The latter corresponded to that flamelet in the calculations of Ref. 13 having the lowest value of strain rate. The strain rate, denoted by the symbol a, is the gradient of the velocity normal to the flame structure, and is a measure of the rate at which reaction products are pulled away in a direction parallel to the reaction sheet. In the base case shown in Figures 2 and 3, it has the value 56.1 sec^{-1}. To investigate optical thickness effects, thicker flamelets corresponding to lower strain rates were synthetically generated by simply stretching the coordinates of the base case by various factors. At the low strain rates, the species profiles correspond nearly to equilibrium values, and it is felt that this approximate procedure will be adequate for illustrative purposes, rather than using the Ref. 12 code to get the exact solution. Characteristic dimension will scale with strain rate approximately as $a^{-1/2}$ (Ref.14). No coupling between radiation and the flame solution is accounted for here; the energy equation in the counterflame solver omits the radiative source term.

Figure 4 shows the total divergence of the radiative flux as a function of position. The position is presented in normalized form to correspond to the coordinates of the base case. For the latter, both the optically thin and thickness-corrected solutions are given. Thickness corrections are seen to be starting to be important for this case. Two other thickness-corrected solutions are given for coordinate stretchings of ten and twenty-five, which correspond to strain rates of .56 and .09 sec^{-1}, respectively. It can be seen that thickness corrections are certainly important for strain rates somewhat lower than 56.1 sec^{-1}. It is in this range that significant temperature reductions relative to the adiabatic case are predicted with optically thin analysis (Ref. 4). Optical thickness effects will cause the temperature reductions to vary somewhat less dramatically with decreasing strain rate.

In a future publication the results of incorporating the analysis presented here into the counterflow flame solver and assessing the impact of radiative loss on NO_x levels will be addressed, and it will be shown that very precise predictions require thickness corrections for low strain rates (Ref. 15). In these calculations the water pure rotational band was left out; it was found that with it the analytic expression (Equation 17) lost accuracy. Equation 5 is also not accurate for this band. Differences of a few percent were found using the exact solution (Equation 16) with and without this band.

Acknowledgements

The author would like to thank J. De Ris for early conversations about wideband models, to L. Chiapetta for providing him with a program to calculate the wideband model parameters, and to A. Vranos for providing the counterflow solutions on which the radiation model was tested.

References

1. M.M. Abu-Romia and C.L. Tien, "Appropriate Mean Absorption Coefficients for Infrared Radiation of Gases", Journal of Heat Transfer, pp. 321-327, 1967.

2. D.K. Edwards and A. Balakrishnan, "Thermal Radiation by Combustion Gases", Intl J. Heat Mass Transfer,Vol. 16, pp. 25-40, 1973.

3. D.K. Edwards, in "Handbook of Heat Transfer Fundamentals", (W.M. Rohsenow, J.P. Hartnett, and E.N. Ganic, eds.), Chapter 14, Part 4, McGraw Hill, 1985.

4. Y. Liu and B. Rogg, "Modelling of Thermally Radiating Diffusion Flames with Detailed Chemistry and Transport", Proceedings of the Eurotherm Seminar No. 17, Heat Transfer in Radiating and Combusting Systems, pp. 114-127, 1990.

5. U.C. Muller, F. Maus, and N. Peters, "Influence of Radiative Heat Loss on Thermal NO- Production in Laminar CO-H2-N2 - Diffusion Flames", poster presentation at Twenty-first Symposium (International) on Combustion, Orleans, France, 1986.

6. A. T. Modak, "Nonluminous Radiation from Hydrocarbon-Air Diffusion Flames", Factory Mutual Research Technical Report 22355-1, 1974.

7. M. Geller, "Tables of Integrals Involving Powers, Exponentials, Logarithms, and the

Exponential Integral", Cal. Tech. Jet Propulsion Lab. Report 32-469, 1963.

8. M. Abramowitz and I. A. Stegun (eds.), "Handbook of Mathematical Functions", Dover Publications, 9th printing, Chapter 6, 1970.

9. J. D. Felske and C.L. Tien, "Infrared Radiation from Non- Homogeneous Gas Mixtures Having Overlapping Bands", JQSRT, Vol. 14, pp. 35-48, 1974.

10. D. K. Edwards and A. Balakrishnan, "Thermal Radiation by Combustion Gases", Int. J. Heat Mass Transfer, Vol. 16, pp. 25-40, 1973.

11. A. T. Modak, "Exponential Wide Band Parameters for the Pure Rotational Band of Water Vapor", JQSRT, Vol. 21, pp. 131-142, 1979.

12. M.D. Smooke, I.K. Puri, and K. Seshadri, "A Comparison Between Numerical Calculations and Experimental Measurements of the Structure of a Counterflow Diffusion Flame Burning Diluted Methane in Diluted Air", Twenty-first Symposium (International) on Combustion/The Combustion Institute, pp. 1783-1792, 1986.

13. A. Vranos, "A Generalized Conditional Scalar Dissipation-Mixture Fraction Joint-PDF for Flamelet Modeling of Non-Premixed Flames", submitted to Combustion Science and Technology, 1991.

14. R. Borghi, "Turbulent Combustion Modelling", Prog. Energy Comb. Sci., Vol. 14, pp. 245-292, 1988.

15. A. Vranos and R.J. Hall, to be published.

Figure Captions

1. Coordinate system for radiation analysis and opposed jet flame geometry

2. Temperature distribution for base case. Strain rate is 56.2 sec-1.

3. Radiating species profiles of base opposed jet case.

4. Radiation source term (divergence of net radiative flux) as function of strain rate.

Figure 1

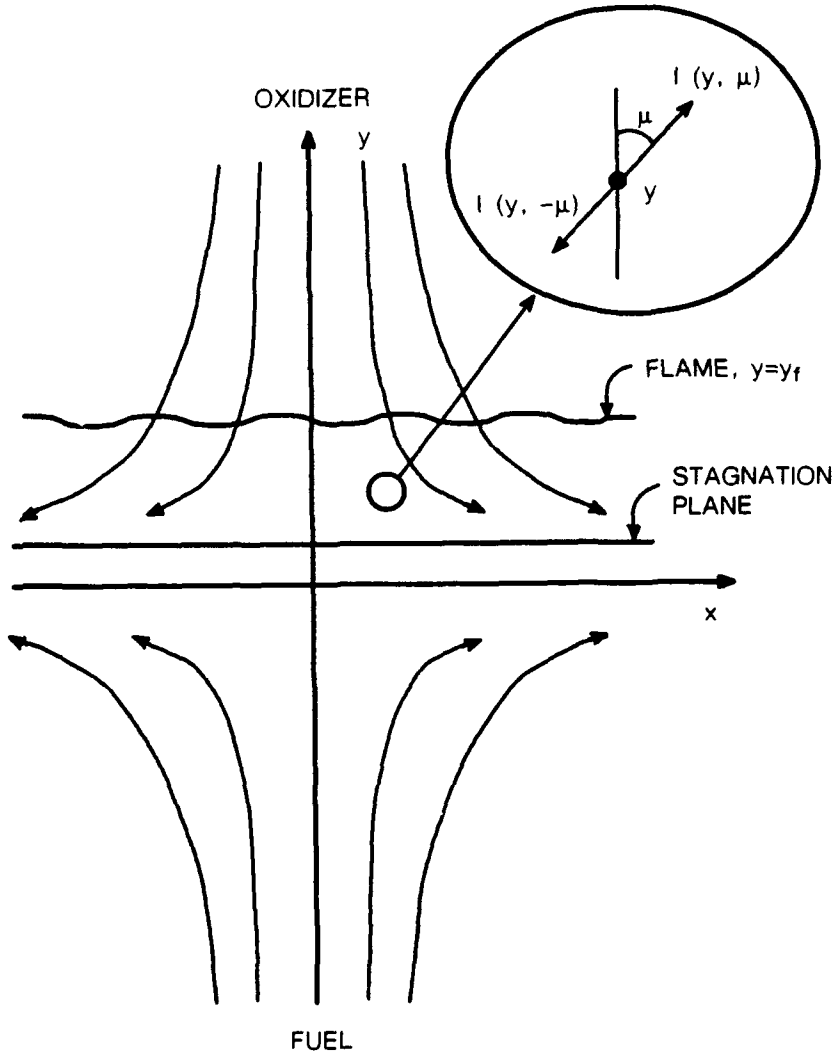

92-4-21-1

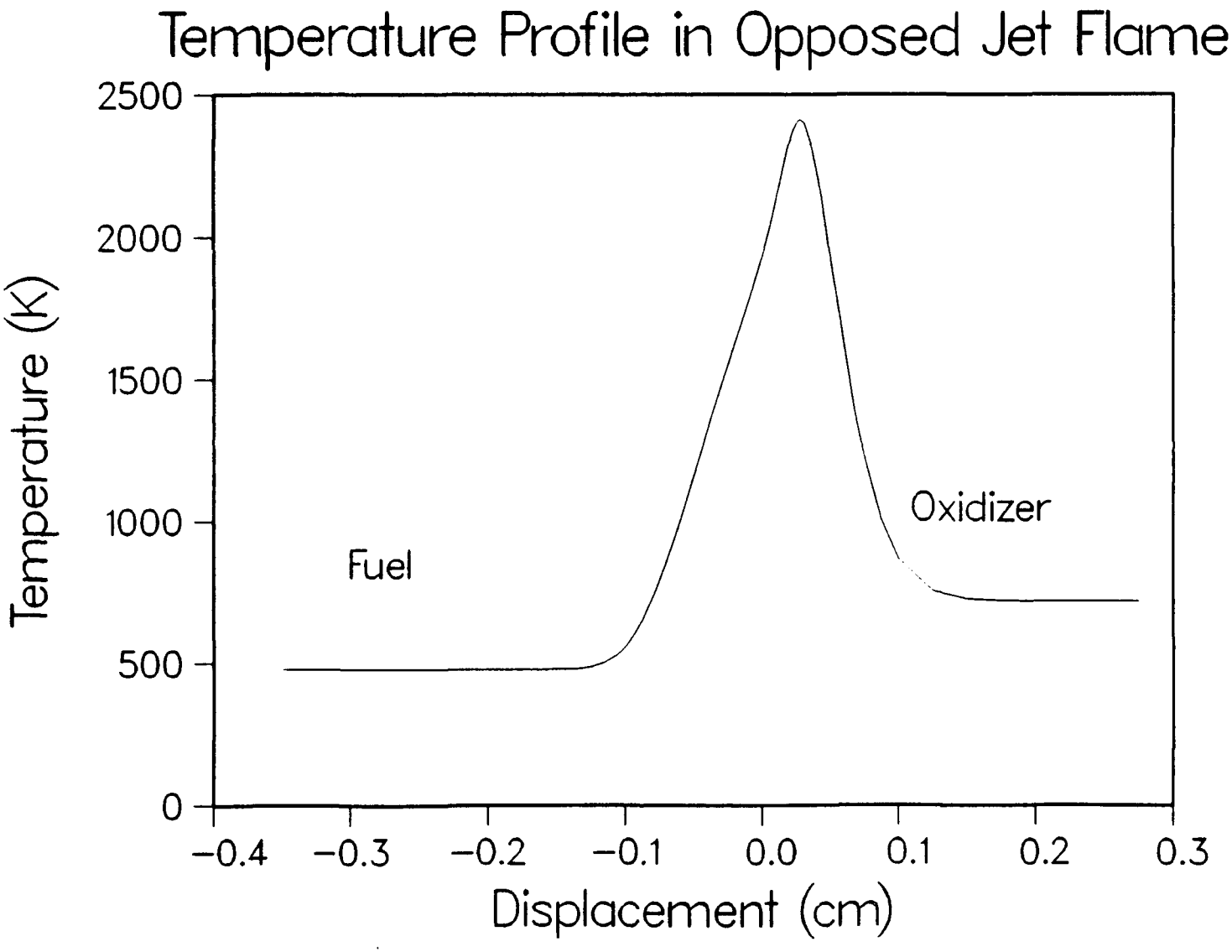
Temperature Profile in Opposed Jet Flame
Temperature (K)
2500
2000
1500
1000
500
0
Fuel
Oxidizer
−0.4
−0.3
−0.2
−0.1
0.0
0.1
0.2
0.3
Displacement (cm)

Figure 2

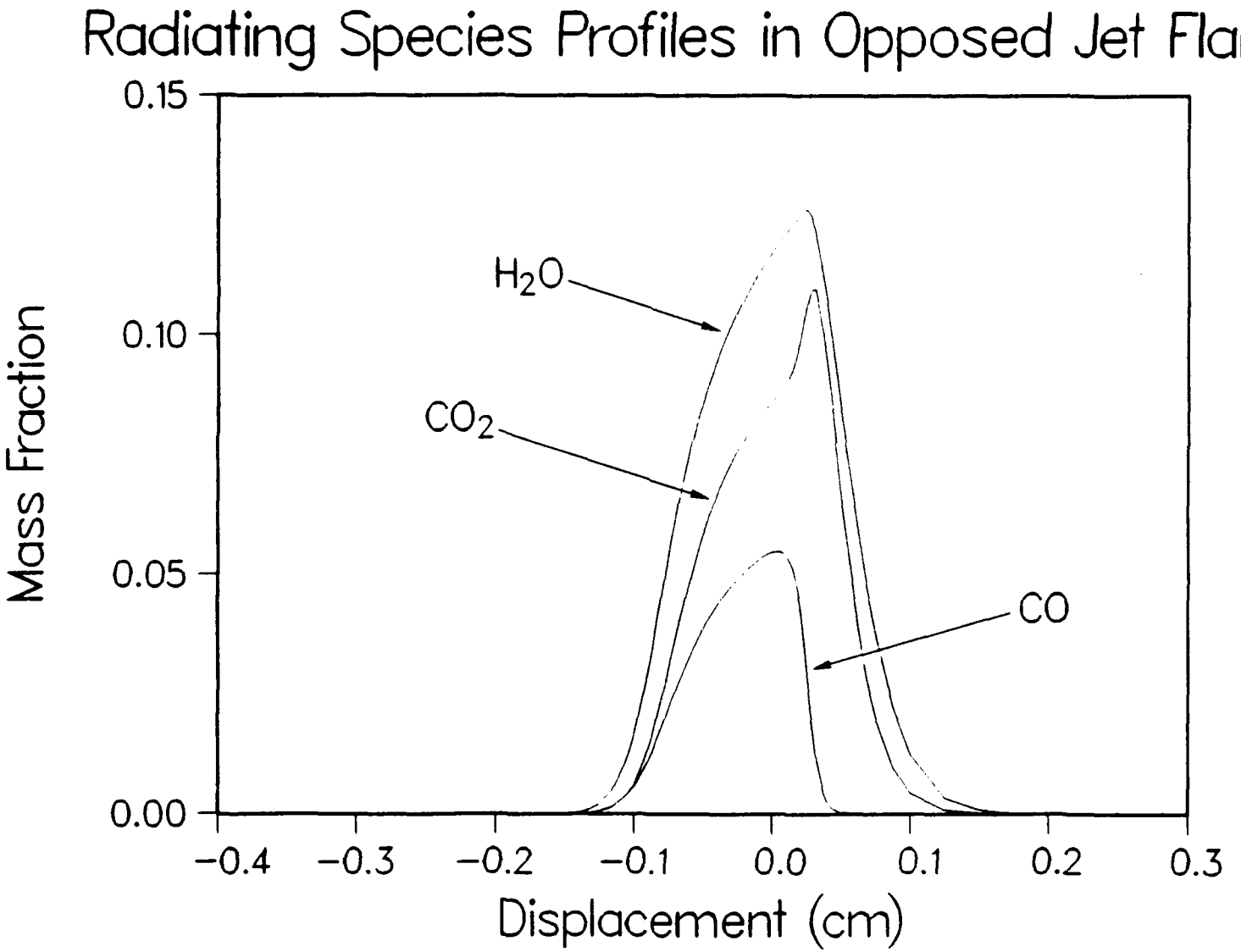
Radiating Species Profiles in Opposed Jet Flame
Mass Fraction
0.15
0.10
0.05
0.00
H_2O
CO_2
CO
−0.4
−0.3
−0.2
−0.1
0.0
0.1
0.2
0.3
Displacement (cm)

Figure 3

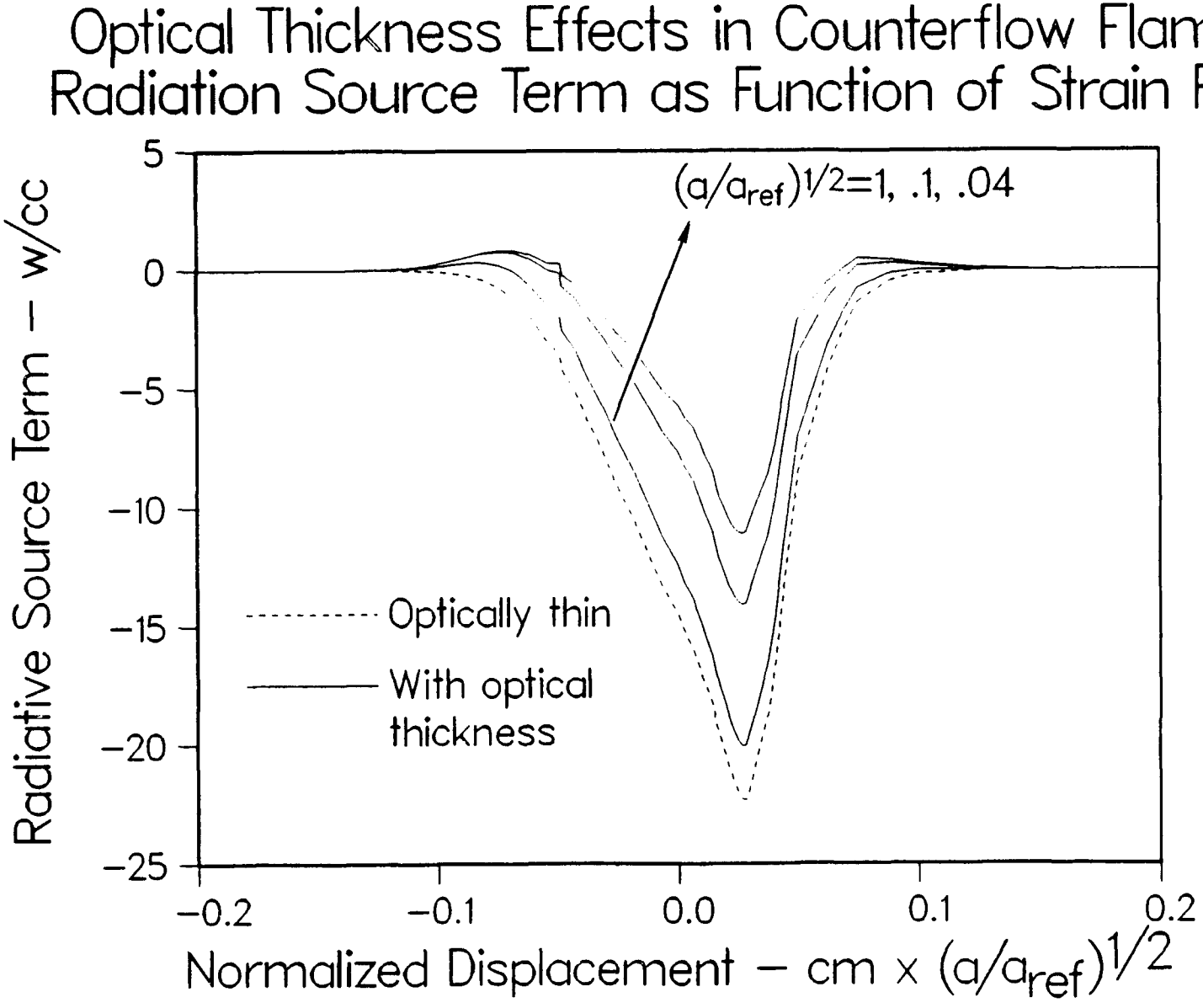
Optical Thickness Effects in Counterflow Flames
Radiation Source Term as Function of Strain Rate
Radiative Source Term – w/cc
5
0
−5
−10
−15
−20
−25
$(a/a_{ref})^{1/2}$=1, .1, .04
Optically thin
With optical thickness
−0.2
−0.1
0.0
0.1
0.2
Normalized Displacement – cm x $(a/a_{ref})^{1/2}$

Figure 4